This is the accepted version of the following article: Etxaniz, A., González-Bullón, D., Martín, C., Alonso, M.T. and Ostolaza, H. (2020), Irreversible *versus* repairable membrane poration: differences in permeabilization elicited by *Bordetella* Adenylate Cyclase Toxin and its hemolysin domain in macrophages. **FEBS J**, 287: 1798-1815, which has been published in final form at https://doi.org/10.1111/febs.15106

Irreversible *versus* repairable membrane poration: differences in permeabilization elicited by *Bordetella* Adenylate Cyclase Toxin and its hemolysin domain in macrophages

Asier Etxaniz[1], David González-Bullón1, César Martín[1], Maria Teresa Alonso[2] and Helena Ostolaza[1#]

From the [1] Departamento de Bioquímica y Biología Molecular (UPV/EHU) and Instituto Biofisika (UPV/EHU, CSIC), Aptdo. 644, 48080 Bilbao, Spain.; [2] Instituto de Biología y Genética Molecular C/Sanz y Flores 3, 47003 Valladolid, Spain

Running title: *Membrane repair upon permeabilization by PFT*

[#]To whom correspondence should be addressed. Dr Helena Ostolaza, Departamento de Bioquímica y Biología Molecular (UPV/EHU) and Instituto Biofisika (UPV/EHU, CSIC), Aptdo. 644, 48080 Bilbao, Spain. gbzoseth@ehu.es ; elenaamaya.ostolaza@ehu.es; Tel.: (34) 946012625; Fax: (34) 946013360; https://orcid.org/0000-0003-2933-9975

Key words : bacterial toxin, pore-forming toxin, membrane permeabilization; membrane repair mechanisms, phagocytes

ABBREVIATIONS

AC, adenylate cyclase domain

ACT or CyaA, Adenylate cyclase toxin-hemolysin

ASM, acid sphingomyelinase

ATP, adenosine triphosphate

BAPTA-AM, 1,2-Bis(2-aminophenoxy)ethane-*N*,*N*,*N*',*N*'-tetraacetic acid tetrakis(acetoxymethyl ester)

BEL, bromoenol lactone

cAMP, cyclic adenosine monophosphate

DMEM, Dulbecco's Modified Eagle Medium

DPA, desipramine

EDTA, ethilen diaminotetraacetic acid

FACS, Fluorescence-Activated Cell Sorting

FBS, fetal bovine serum

FITC, fluorescein iso-thiocyanate

Fura2-AM, Acetoxymethyl 2-[5-[bis[(acetoxymethoxy-oxo-methyl)methyl]amino]-4-[2-[2-[bis[(acetoxymethoxy-oxo- methyl)methyl]amino]-5-methyl phenoxy]ethoxy]benzofuran- 2-yl]oxazole-5-carboxylate

GMFI, Geometric mean fluorescence intensities

HBSS, Hank's balanced salt solution

ICP–AES, inductively coupled plasma atomic emission spectroscopy

LDH, lactate dehydrogenase

MAb, monoclonal antibody

PBS, phosphate buffered saline

PFT, pore-forming toxin

PI, propidium iodide

PKA, protein kinase A

PLA, phospholipase A

PPADS, pyridoxalphosphate-6-azophenyl-2',4'-disulfonic acid

RTX, Repeats in ToXin

SLO, streptolysin O

TLC, thin layer chromatography

TX-100, Triton X-100

ABSTRACT

Rapid plasma membrane repair in response to pore-forming toxins is crucial for cell survival, but the molecular mechanisms employed by eukaryotic nucleated cells to maintain membrane integrity and the specificities of such pathways remain poorly understood. Here we have explored the permeabilization elicited by the *Bordetella pertussis* Adenylate Cyclase Toxin (ACT), a 200 kDa protein toxin with α-helical pore-forming domain that forms pores of tunable size, and evaluated the response of target macrophages to such toxin poration. We show here that the response and the fate of target macrophages depend on toxin pore width. We find that the toxin´s hemolysin moiety induces a transient membrane permeabilization by forming wide enough pores allowing Ca^{2+} influx into the target cell cytosol. This activates a Ca^{2+}-dependent cellular response involving exocytosis and endocytosis steps eliminating toxin pores and restoring membrane integrity. In contrast the full length native toxin, at low concentrations, forms very small pores that cause insidious perturbation of cell ion homeostasis that escapes control by the macrophage membrane repair response, eventually leading to cell death. Our data reveal that permeability to Ca^{2+} and ATP are key elements in the membrane repair pathway for eliminating α-helical pores of bacterial origin.

Key words : bacterial toxin, pore-forming toxin, membrane permeabilization; membrane repair mechanisms, phagocytes

INTRODUCTION

Several pathogenic bacteria use pore-forming proteins to directly damage cells, introduce virulence factors into the cytosol of target cells [1], or promote bacterial intracellular growth [2]. Interestingly, nucleated cells are able to repair the perforated plasma membrane, recovering its structural and functional integrity, whereas removal of small pores does not always involve Ca^{2+} influx and exocytosis-endocytosis processes, and can be achieved by exocytosis of the pores [3]. To date, recovery of plasma membrane integrity has been noted in cells permeabilized by toxins that form β-barrel pores, either large ones, such as those formed by streptolysin O [4], pneumolysin [5] or listeriolysin [6], as small ones, such as the ones formed by *Staphylococcus aureus* α-hemolysin [3] or by *Photobacterium damselae* phobalysin [7]; it occurs in various cell types in culture, and has been shown to operate *in vivo* in *Caenorhabditis elegans* [8]. Repair of injured plasma membrane is also activated after physical or mechanical wounding or upon permeabilization by large pore-forming complexes formed by perforin or by complement [9]. Repair of the large lesions appears to be Ca^{2+}-dependent and involve subsequent steps of lysosomal exocytosis and endocytosis of the pore-ridden membrane [10-12], whereas Ca^{2+}-dependent repair of small beta-pores has been shown so far only for the comparably large phobalysin pore [7]. By contrast, repair pathways activated by pore-forming toxins that form pores of alpha-structure, large or small, are not known.

Adenylate cyclase toxin-hemolysin (ACT, also dubbed CyaA, or AC-Hly) is an important virulence factor secreted by *Bordetella pertussis*, and it has a critical role in the early stages of respiratory tract colonization by this pathogenic bacterium [13,14]. ACT belongs to the so-called RTX (Repeats in ToXin) family of proteins characterized by

possessing in their C-terminal sequence a variable number of glycine and aspartate-rich repeats of nine amino acids [15], mostly exhibiting cytotoxic/cytolytic pore-forming activity [15,16] . ACT is a single polypeptide of 1706 amino acids, that is unique among its relative RTX cytolysins in that, besides the characteristic pore-forming RTX hemolysin (Hly) domain (residues ≈500-1706), it has an N-terminal enzymatically active adenylate cyclase (AC) domain (≈ residues 1-400) [17] which is delivered by the RTX hemolysin domain into the target cell cytosol. The toxin exhibits besides, intrinsic phospholipase A (PLA) activity, necessary for AC translocation [18,19]. The RTX hemolysin domain contains, in turn, a membrane-interacting hydrophobic region with amphipathic-hydrophobic α-helixes (∼500-750 residues), two conserved Lys residues (Lys 863 and Lys 913) that are post-translationally fatty acylated by a dedicated acyltransferase (CyaC), and a C-terminal secretion signal recognized by a specific secretion machinery (CyaB, CyaD and CyaE) [17,20,21]. The toxin segment extending approximately from residue 400 to 500, that connects the catalytic AC domain to the pore-forming RTX hemolysin domain, has been recently revealed that might be involved in translocation of the AC domain across the cell membrane, assisting membrane insertion [22,23] and it has also been proposed that negatively charged residues of that segment restricts the membrane-permeabilizing capacity of adenylate cyclase toxin [24]. All ACT activities depend on the covalent fatty acylation of pro-ACT, and on the binding of Ca^{2+} ions to the numerous sites formed in the RTX domain by the glycine- and aspartate-rich repetitions [21,25,26].

ACT primarily targets host myeloid cells expressing the CD11b/CD18 integrin, which acts as specific receptor for the toxin in these cells [27], and upon receptor binding,

the RTX hemolysin domain inserts into cellular membranes and mediates in AC domain translocation *via* membrane restructuring induced by toxin´s intrinsic PLA activity [19,28]. Once inside the target cytosol, the AC domain binds calmodulin and catalyzes the conversion of ATP into cAMP [20] thereby subverting cellular signaling and leading eventually to cell death. For long time the toxic effect of ACT on host macrophages has been attributed only to this supraphysiological production of cAMP [29]. However, ACT exhibits also a low haemolytic phenotype on mammalian erythrocytes [30,31] presumably by forming small membrane pores by its helical hydrophobic segment, that permeabilize cells [32,33], and recent work suggests that this pore-forming activity is sufficiently potent to cause also lysis of target $CD11b^+$ cells and that it contributes to overall cytotoxicity of CyaA toward phagocytic cells [34].

Evidence for pore formation by ACT mainly came through biophysical studies with artificial membranes and osmoprotection assays with erythrocytes [32,33,35], and from such studies ACT was reported to form small cation-selective pores of 0.6-0.8 nm of diameter and short life-time [32]. Several studies have indicated that the hemolytic pore-forming activity of ACT is elicited by toxin oligomers, whereas translocation of the catalytic domain into cell cytosol appears to be a linear function of toxin concentration, suggesting that monomers of ACT may deliver the AC domain across membrane [33,36,37]. The permeabilization properties of ACT on nucleated cells are much less known.

Recently, our laboratory showed that upon translocation of the catalytic domain and ulterior cleavage of the full length ACT by cellular calpains, the AC domain is released into the cytosol of target macrophages, while a C-terminal ACT fragment (residues ≈482-1706) remains into the membrane [38]. At present, it is not known whether

a possible accumulation of this fragment permeabilizes the plasma membrane of target phagocytes, or which other can be the cellular consequences of it.

This study was aimed to investigate in detail the process of membrane permeabilization of target macrophages by these two proteins, full length intact ACT and the RTX-hemolysin protein form, and to explore whether in the injured cells membrane repair responses are activated, in the likeness to beta-barrel pore-forming toxins. To this goal we used a truncated ACT hemolysin mutant, ACT-ΔN482, extending from amino acid 483 to 1706 of the ACT sequence, thus resembling the RTX ACT hemolysin domain that can be found *in vivo* in the target cell membrane. We find here that both proteins permeabilize differently the cell membrane of target cells: pore-formation by the ACT hemolysin moiety is repairable, whereas the full-length ACT induces an irreversible membrane permeabilization that may eventually lead to cell death.

MATERIALS AND METHODS

Expression and purification of full length ACT and ACT-ΔN482 mutant protein

ACT was expressed in *Escherichia coli* XL-1 blue cells (Stratagene) transformed with pT7CACT1 plasmid, kindly provided by Dr. Peter Sebo (Institute of Microbiology of the ASCR, v.v.i., Prague, Czech Republic) and purified as described in Karst et al [39].ACT- ΔN482 was expressed in *Escherichia coli* XL-1 blue cells (Stratagene) transformed with pCyaAC-PF plasmid, kindly provided by Dr. C. Angsuthanasombat and Dr. B. Powthongchin (Laboratory of Molecular Biophysics and Structural Biochemistry, Institute of Molecular Biology and Genetics, Mahidol University, Thailand) and purified following the same protocol as for ACT [39].

Cell culture

J774A.1 macrophages (ATTC, number TIB-67) were grown at 37°C in DMEM containing 10% (v/v) FBS, and 4 mM L-glutamine in a humidified atmosphere with 5% CO_2.

Determination of protein endocytosis by FACS

Internalization of ΔN482 in J774A.1 cells was determined by flow cytometry as previously described, [40] with minor modifications. Geometric mean fluorescence intensities (GMFI) were used to calculate the ΔN482 internalization time course. Briefly, macrophages were from one side incubated with ACT-ΔN482 hemolysin (5 nM) for 10 min at 4ºC to determine total toxin binding to the cell membrane (no internalization occurs at this low temperature). From other side, cells were firstly incubated at 4ºC 10 min to allow toxin binding, then, washed 3 times with ice-cold PBS to remove unbound toxin, and then incubated at 37°C for various time intervals (0 - 30 min). After each incubation time cells were then washed, fixed for 10 min in 3,7 % paraformaldehyde, and detached in ice-cold PBS, labeled under non-permeabilizing conditions against ACT-ΔN482 with the appropriate antibody (monoclonal MAb 9D4) for 1 h at room temperature, then centrifuged, washed and mixed in buffer containing FITC-conjugated secondary antibodies and incubated for 1 h at room temperature. Then, cells were washed, resuspended in ice-cold PBS and analyzed in a FACSCalibur flow cytometer (Beckton Dickinson). GMFI values determined at 4ºC after the initial 10 min incubation and subsequent cell washing and labeling was taken as total binding (100% toxin bound to the cell membrane). GMFI values determined after the corresponding incubations at 37ºC were taken as the amount of toxin remaining at the plasma membrane (non-internalized) after each incubation period (0-30 min). Then, the percentage of ΔN482 internalization at

each time point (0-30 min) was calculated subtracting to the total binding (GMFI at 4ºC) the GMFI value of the cells incubated at 37ºC.

Confocal Microscopy

Cells were grown to sub-confluency on to 12 mm diameter glass coverslips placed into the wells of a 24-well plate. ACT-ΔN482 (1 and 10 nM) was added to the medium and cells were incubated for 5 min at 37ºC. Then, treated cells were washed three times in PBS to remove unbound toxin, fixed for 10 min with 3.7% paraformaldehyde and permeabilized with acetone at –20 °C. Control cells followed the same procedure. Then samples were incubated for 1h with the appropriate primary antibodies: anti-ACT 9D4 monoclonal antibody(Santa Cruz Biotechnology Inc, Germany) and mouse anti-CD11b antibody (RM 2800, Invitrogen) (for labelling of the CD11b/CD18 ACT receptor in macrophages), followed by incubation the corresponding secondary antibodies Alexa-488 labelled secondary antibody for ACT MAb, or goat anti-rat Alexa-Fluor 633 conjugated secondary antibody (Thermofisher, A-21-094) for CD11b antibody Coverslips were mounted on a glass slide and samples were visualized using a confocal microscope (Olympus IX 81) with sequential excitation and capture image acquisition with a digital camera (Axiocam NRc5, Zeiss). Images were processed with ImageJ software.

Propidium Iodide (PI) permeability assay

J774.A1 cells were cultured on 6 well plates at 60% confluence and incubated with different toxin concentrations for 5 min at 37 °C to allow irreversible binding of toxin to the cells. Then, cells were washed to remove unbound toxin, and incubation again at 37 °C for various intervals (0, 5, 10, 30, 60, 120 min). After each incubation time, cells were stained for 4 min with PI 50 µg/ml (Sigma-Aldrich), to asses pore formation and membrane repair, as described previously [11]]. PI incorporated into cell

was analyzed in a FACSCalibur flow cytometer (Beckton Dickinson). Controls were performed with vehicle buffer. After flow cytometry (FACSCalibur; BD) of at least 10,000 cells, % of PI positive cells was quantified and the data were analyzed using Flowing Software. Controls were performed with vehicle buffer alone.

Release of LDH from J774A.1 cells

Cells were incubated with the corresponding protein toxin (ACT or ACT-ΔN482) in OPTIMEN buffer and LDH release from cells was determined by the lactate dehydrogenase (LDH) release assay, using the LDH Cytotoxicity assay kit (Innoprot, Spain) and percentage of LDH release was calculated as (extracellular LDH/total LDH released upon cell permeabilization with TX-100) x 100.

Determination of β-hexosaminidase activity

β-Hexosaminidase secretion assays, which reflect extracellular accumulation of the enzyme resulting from sustained lysosomal exocytosis, were performed as previously described [41]. J774A.1 cells were cultured in 24 well plates and after toxin treatment, 350 µl of the cell supernatant was incubated for 15 min at 37°C with 50 µl of 6 mM 4-methylumbellyferil-N-acetyl-β-D-glucosaminide (Sigma) in sodium citrate-phosphate buffer, pH 4.5. The reaction was stopped by addition of 100 µl of 2 M Na_2CO_3 and 1.1 M Glycine, and the fluorescence was measured in FluoroMax 3 fluorometer with excitation at 365 nm and emission at 450 nm. The percentage of cellular β-hexosaminidase that had been secreted was calculated relative to total enzyme content of the cell that is released with Triton X-100 treatment.

Measurement of Intracellular [Ca^{2+}]

J774A.1 cells grown on glass coverslips were loaded with 2 µM Fura2-AM (Thermo Fisher) for 30–40 min in DMEM at room temperature in the dark, and washed in

20 mM Tris-HCl, 150 mM NaCl, 2.4 mM $CaCl_2$, 10 mM glucose, pH 7.4. The cell-containing coverslips were mounted on a thermostatized perfusion chamber under a Nikon Diaphot microspectofluorometer and visualized with a 40 oil-immersion fluorescence objective lens. Test solutions were applied by continuous perfusion at 2-3ml/min. For fluorescence measurements, cells were alternately epi-illuminated at 340 and 380nm and light emitted above 520-nm was recorded using a Hamamatsu Digital Camera C4742-98handled by Simple PCI 6.6 Hamamatsu software. Consecutive frames obtained at 340 and 380nm excitation were rationed pixel by pixel using imageJ software and calibrated in $[Ca^{2+}]$ by comparison with Fura-2 standards.

Determination of cytosolic potassium levels by ICP–AES

Incubation of cells in HBSS without K^+ with the indicated working concentrations of ACT and ACT-ΔN482 was carried out for different times. The cells were washed three times with PBS and lysed with 500 µl of deionized water. The lysed cells were centrifuged (20 min, 4 °C, 40,000 x g) to remove the membranes. Diluted solutions (0.7 ml) were acid digested with 0.1 ml of HNO_3 (concentrated) for 12h in order to eliminate any carbon interference in the analytical determination. For total K^+ concentration characterization in extracts, optical emission spectrophotometer with inductively coupled plasma (Horiba Jobin Yvon, Activa) was employed using a quartz Meinhard concentric nebulizer, a Scott-type spray chamber and a standard quartz sheath connection between the spray chamber and the torch. Mean values were reported from 766.491 nm and 769.897 nm wavelengths.

Lipid extraction and quantification of ceramide by Thin Layer Chromatography

J744A.1 macrophages were labeled with $[H^3]$ palmitic acid overnight at 37°C. Cells then were incubated with ACT-ΔN482 (20 nM) for 10 minutes at 37°C, washed in

ice-cold PBS with 5 mM EDTA and scraped into 1 mL of methanol. The lipids were extracted adding 1 ml of chloroform and 0.9 mL 2 M KCl + 0.2 M HCl. Chloroform phase was dried under nitrogen and ceramides were separated by TLC using Silica Gel 60 plates developed with chloroform:methanol:acetic acid 9:1:1 and then dried. Plates were re-developed in petroleum ether:diethylether:acetic acid 60:40:1, dried and stained with iodide vapour. Radioactive ceramides were quantified by scraping from TLC plates followed by liquid scintillation counting.

Statistical Analysis

All measurements were independently performed at least 3 times, with n=3 unless otherwise stated, and results are presented as mean ± s.d. Levels of significance were determined by a two-tailed Student´s *t* test, and a confidence level of greater than 95% ($p<0.05$) were used to establish statistical significance.

RESULTS

Pemeabilization of macrophages by ACT and ACT-ΔN482 hemolysin

To assess the permeabilization capacity of ACT and ACT-ΔN482 hemolysin on phagocytes (J774A.1 macrophages) we used the membrane-impermeable propidium iodide (PI) method. **Fig 1A** shows original histograms of phagocytes exposed to vehicle buffer (control), to ACT-ΔN482 (2.5 nM) or to ACT (2.5 nM) at 37°C for 10 min and then immediately incubated with PI (50μg/ml) for 4 min. Relative to control untreated cells (PI-positive ≈10%), ACT-ΔN482 hemolysin made ≈75% of the phagocytes PI-positive (**Fig.1A)**. Since PI dye does not cross intact membranes, the most likely and simple explanation for the rapid nuclear DNA staining with PI is that PI-permeable hemolysin pores are formed on the plasma membrane that allow the dye entry into the cells, and thus it would indicate that ACT-ΔN482 hemolysin permeabilizes macrophages

through pore formation. By contrast, macrophages exposed to the full length ACT at the same concentration (2.5 nM) did not result permeable to PI (**Fig. 1A**), and required concentrations above 50 nM to induce significant membrane permeabilization to PI in incubations of 10 min (**Fig. 1B)**, whereas for the same incubation period ACT-ΔN482 permeabilized the macrophages for PI at concentrations even below 1 nM (**Fig. 1B**). We hypothesized that the almost null cell PI staining upon ACT treatment might be due to formation of very small, PI-impermeable pores by ACT at the toxin concentrations used. Assuming that the apparent hydrodynamic radius of PI is ≈ 1.0 nm, it can be concluded that in the conditions assayed the lesions formed by ACT in the membrane of macrophages are smaller than 1.0 nm, whereas ACT-ΔN482 forms pores larger than 1.0 nm. The haemolytic capacity of both toxins was also checked on sheep erythrocytes (Fig 1C) observing that wt ACT has a more modest lytic potency as compared to the ACT-ΔN482 hemolysin variant. These data agree with a previous study in which other ACT-hemolysin construct, ΔN489 (aa 6 to 489 of wt ACT sequence deleted), very similar to our ACT-ΔN482 mutant, was reported to be hemolytically much more active than the full length ACT [42,43].

ACT-ΔN482 hemolysin elicits permeability to K^+ and Ca^{2+} ions, whereas intact ACT, at low concentrations, permeabilizes the phagocytes to K^+, but only slightly to Ca^{2+}

Since the use of PI seemed not to be a good reporter method to follow cell permeabilization by ACT, we checked for toxins-induced influx-efflux of K^+ and Ca^{2+}, as permeability to these ions, particularly to K^+, is a hallmark of the permeabilization by all pore-forming toxins investigated so far [6]. Variations of the intracellular [K^+] were quantified using the inductively coupled plasma atomic emission spectroscopy (*ICP*-

AES), and the possible Ca^{2+} dynamics were measured by fluorescence microscopy, with the calcium-sensitive probe Fura-2-AM.

Treatment of macrophages with ACT-ΔN482 hemolysin at 37°C and concentrations in the range 0.1-1.0 nM caused a dose-dependent loss of cellular K^+ in a timescale of a few minutes (0-10 min) (**Fig 2A)**, and similarly, we measured a dose-dependent increase in the cells Ca^{2+} concentration (**Fig. 2C**), within several minutes upon exposition of Fura-2-AM- loaded J774A.1 macrophages to ACT-ΔN482 (0-5 nM), achieving maximal values within 3-4 min for the highest toxin dose tested (5 nM). In both cases, the time courses for K^+ efflux and Ca^{2+} entry induced by this hemolysin variant were fully consistent with the time scale of membrane permeabilization determined formerly by the PI penetration method (**Fig 1A**), suggesting again that most likely all these solutes move through pores formed by the ACT-ΔN482 hemolysin in the macrophage membrane. The full length ACT, in contrast, required about 10-30 times greater concentrations (2.5-30 nM) for inducing in the same time scale a K^+ efflux similar to the observed for the ACT-ΔN482 hemolysin (**Fig. 2B**), and something similar happened with the Ca^{2+} entry (**Fig. 2D**), at least six fold higher ACT concentrations (≈30 nM) were required to induce a Ca^{2+} entry comparable to that elicited by ACT-ΔN482 hemolysin (≈5.0 nM). At lower ACT concentrations (1.0 and 5.0 nM) the Ca^{2+}influx was very subtle and at concentrations below 1.0 nM no Ca^{2+} entry was detectable by the fura-2 method (not shown). These data were thus consistent with the PI results (**Fig 1**) and indicated that relative to the ACT-ΔN482 hemolysin variant, the full length ACT requires higher concentrations to induce a similar rapid (a few min) permeability to K^+, and Ca^{2+} in phagocytes, supporting the hypothesis that ACT at low doses (and low incubation

times) forms small lesions (<1.0 nm), whereas at these same conditions, the ACT-ΔN482 pores seem to be larger than 1.0 nm.

To be sure and be able to affirm that the ion fluxes we have detected for both ACT and ACT-ΔN482 in the phagocytes took place through pores formed by these toxins in the cell membrane and not by other means (for example, by activation of other endogenous channels), we performed a series of control experiments. Our laboratory had previously documented that ACT, at high concentrations, can induce the opening of PKA-activated L-type Ca^{2+} channels through its cAMP-generating activity [44] , and since Ca^{2+} elevations can also activate K^+ releases, we checked whether this could be the source of the observed K^+ exit in the ACT-treated macrophages. To this aim we preincubated the cells with two inhibitors of PKA-activated L-type Ca^{2+} channels, namely, nifedipine (10 μM; inhibitor of L-type Ca^{2+} channels, Sigma) and KT5720 (56 μM; Inhibitor of PKA, Sigma). As shown in the **Fig 2E** none of these two inhibitors had any significant effect on the ACT-induced K^+ efflux, thus discarding that the observed efflux of this monovalent cation induced by ACT was related to calcium-activated K^+ fluxes. Therefore, excluded the involvement of the L-type Ca^{2+} channels, we concluded that the observed K^+ release in the ACT-treated phagocytes takes place most likely through K^+ permeable ACT pores . An ACT-induced K^+ efflux had been previously reported by others from both $CD11b^+$ cells such as macrophages, and also from erythrocytes [37,45]. Regarding the ACT-ΔN482 hemolysin, we discarded a possible intervention of PKA-activated L-type Ca^{2+} channels in the Ca^{2+} transients induced by this hemolysin in phagocytes, since nor nifedipine nor KT5720 had any effect on the Ca^{2+} entry (**Fig 2F**). This was indeed expected, given that the ACT-ΔN482 mutant polypeptide lacks the cAMP-producing AC domain and cannot thus produce cAMP. Finally, and because it has been reported that

bacterial toxin pores can, in some instances, be associated with an ATP release that might activate purinergic channels present at the plasma membrane, that would enhance cell permeabilization and contribute to Ca^{2+} entry into cells [46], we performed a control experiment using PPADS (pyridoxalphosphate-6-azophenyl-2',4'-disulfonic acid, Sigma), a selective antagonist of P2X-type purinergic channels. Fig **2G** shows a representative experiment in which cells were preincubated with PPADS at three different concentrations (20, 100 and 200 μM), that has been shown to be effective in inhibiting purinergic channels [46], and then exposed to ACT-ΔN482 (2.5 nM) (Fig **2G**, panel A). Though a faint reduction in the maximal amplitude of the signal was observed in the PPADS-treated cells, this inhibitor did not avoid the rapid and robust Ca^{2+} influx induced by the hemolysin (**Fig 2G**), being thus proven that the ACT-ΔN482 hemolysin induces in macrophages Ca^{2+} fluxes independently of a possible activation of purinergic channels. In sum, our results demonstrated that ACT-ΔN482 hemolysin at low concentrations permeabilizes the plasma membrane of target macrophages to both K^+ and Ca^{2+}, independently of L-type Ca^{2+} channels and of purinergic channels, and so it can be concluded that at the toxin concentrations assayed, the ACT-ΔN482 hemolysin forms most likely K^+- and Ca^{2+}-permeable pores. Conversely, the full length toxin ACT, at low physiologically relevant concentrations (≤ 1.0 nM) [47] permeabilizes the cell membrane mainly to K^+, which might be consistent with the reported small size of the ACT pores (0.6-0.8 nm)[32], while at these low doses permeability to Ca^{2+} by ACT is very faint, perhaps resulting only from its adenylate cyclase activity and concomitant cAMP production that could activate PKA-dependent L-type Ca^{2+}channels, as we demonstrated in other previous study [44]. Larger toxin doses seem to be required to induce a more robust Ca^{2+} entry.

Notwithstanding the foregoing, we do not discard that in other conditions, at higher hemolysin doses and longer incubation times, a possible contribution of purinergic channels might exist and can contribute more relevantly, since other authors have found recently that in the permeabilization of erythrocytes by a similar ACT hemolysin (ΔN489), purinergic channels seemed to contribute to the final hemolysis extent when the ΔN489 concentration used was above 5 nM [43].

Macrophages permeabilized by ACT-ΔN482 hemolysin reseal their plasma membrane, but permeabilization by full length ACT is not repaired

To investigate whether ACT or ACT-ΔN482 hemolysin-treated macrophages were able to recover the damaged membrane, and settle the optimum experimental conditions to observe it by flow cytometry, we treated J774A.1 cells with ACT or ACT-ΔN482 hemolysin (2.5 nM) in two different conditions, one , in which the toxin remained present in the medium for all the incubation periods ("constant"), and other, in which cells were exposed to toxin for a brief period of time (5 min) ("pulse"), then washed with fresh medium, and then incubated for different additional times (0-30 min) to follow their progress. In both sets of experiments, after each incubation time, a solution of propidium iodide (PI) was added to the cells and left for additional 4 min, after which cells were analyzed in a flow cytometer. **Fig. 3A** shows the results obtained with both incubation methods for ACT-ΔN482. When the hemolysin was permanently present for all the incubation period (0-30 min) it was observed that after only 5 min about 78% of the cells became pemeabilized to PI, and this percentage remained more or less constant after the longer incubation periods (10 and 30 min), suggesting that at such toxin exposition condition cells were not able to cope with the membrane damage inflicted. By contrast,

when cells were exposed to ACT-ΔN482 hemolysin for a brief pulse (5 min), and left to recover, for different times, analysis by flow cytometry revealed that during the first 5 min after toxin incubation there was a pronounced increase in the number of cells that became PI positive (≈77%), and thus permeabilized, as propidium iodide penetrated into the treated cells, proportionally to the ACT-ΔN482 concentration tested (0-2.5 nM) (**Fig 3A** and **3B**). After longer incubation periods (≥10 min) however, cells became progressively impermeable to PI (**Fig 3A**) with values close to control cells after 30 min recovery. From these data we surmised that inability of PI to enter into cells reflected a membrane resealing process. To rule out artifactual conclusions, i.e. that cells that were PI-positive at short times died, and thus were not detected after 30 min, the same experiment was performed but with PI present from the beginning, before toxin addition and for the entire incubation time. Under these conditions it was clearly observed that cells that became PI-positive at short times (5 min) remained PI-positive after 30 min, though their membrane has been repaired (**Fig 3C).** In a parallel control assay we confirmed that in the assay conditions cell viability (measured as LDH release) of the PI-permeable hemolysin-permeabilized cells was preserved (**Fig 3D**). On this basis we concluded that macrophages permeabilized by ACT-ΔN482 were able to reseal the perforated plasma membrane after moderate damage by the toxin.

On the contrary, macrophages exposed to a similar short pulse (5 min) of wt ACT (5 nM) showed a very different behavior (**Fig. 3E**), since a PI staining was only detectable very late, after a rather long time (≈1h) from the short toxin pulse, and increased progressively and slowly with time (**Fig. 3E**) most likely due to a progressive increase in cell mortality, as judged by the parallel progressive increase in the LDH release (**Fig 3F**). To discern if following the ACT pulse of 5 min the cell membrane

remained permeabilized till PI-permeable lesions developed, or a very rapid membrane resealing could have been taken place that would explain the initial negative PI-staining, we quantified the ACT-induced K^+ efflux at 0', 5', 15' 30', 60'and 120' after an initial 5' ACT (5 nM) pulse, as better reporter of membrane permeabilization. As depicted in **Fig 4** it was observed that following the short ACT pulse there was a continuous decay of the intracellular K^+ content for ≈30 min achieving a plateau value of about ≈50% of intracellular K^+, that remained constant for the remaining ≈3h of incubation. These results indicated that after the toxin pulse (pore formation) the permeability to K^+ was maintained for all the incubation time period, and thus it could be excluded that the absence of an early PI staining in the ACT-treated cells could be related to a very rapid membrane resealing. Very likely thus, cells treated with ACT (5 nM) became permeable to PI at the time that became also permeable to LDH, this is at dying. In contrast, in the cells under the ACT-ΔN482 pulse there was a rapid continuous lose of K^+ for the first 30 min post-treatment, but then the intracellular K^+ concentration could partially recovered (**Fig 4**), consistently with an activation of a membrane repair process as inferred from **Fig 3**. From these data we concluded that the macrophages permeabilized by ACT-ΔN482 hemolysin reseal their plasma membrane, whereas permeabilization by full length ACT is not repaired.

Extracellular Ca^{2+} influx and ATP are necessary for membrane resealing in phagocytes permeabilized by ACT-ΔN482 hemolysin

To determine whether restoration of the membrane integrity in cells permeabilized by ACT-ΔN482 hemolysin could rely on Ca^{2+}, we performed the same assay as the described in Fig 3, but pre-incubating the phagocytes firstly for 60 min with BAPTA-AM (50 μM, Thermo Fisher), a cell-permeable Ca^{2+}-chelating agent, to assure that there are no

cytosolic Ca^{2+} transients and Ca^{2+} is clamped at low levels. As shown in **Fig 5A,** the cells that had been exposed directly to the ACT-ΔN482 hemolysin without BAPTA preincubation showed a post-permeabilization resealing process. By contrast, in cells pretreated with BAPTA and then exposed to ACT-ΔN482 hemolysin (2.5 nM), penetration of PI to the cell interior increased continuously along the time, suggesting that in absence of Ca^{2+} increases, cells cannot restore cell membrane integrity. From this we concluded that the membrane repair mechanism activated in phagocytes by ACT-ΔN482 hemolysin is Ca^{2+}-dependent. We include a control experiment showing that in cells pre-treated with the calcium chelator BAPTA no calcium rise is detected into the cell cytosol upon ACT-ΔN482 toxin treatment (**Fig 5B**).

Since exocytosis-endocytosis-based membrane repair pathways require both, Ca^{2+} and energy [11] we checked whether ATP was also necessary. To this aim we exposed J774A.1 cells preincubated with sodium azide and 2-deoxy-D-glucose (Sigma) in glucose-free medium to ACT-ΔN482. As shown in **Fig. 5C**, the ATP depleted cells were not able to repair the membrane permeabilized by the ΔN482- hemolysin (2.5 nM), in spite of that the ΔN482- hemolysin induced the same Ca^{2+} influx as before (not shown), proving thus that ATP depletion impedes membrane resealing. The data in **Fig 5** demonstrate, therefore, that ATP and Ca^{2+} are both necessary to trigger a membrane reseal pathway and cope with membrane permeability. On this basis, thus, the incapability of the full length toxin, ACT, to promote membrane resealing can be explained by the consumption of ATP by the adenylate cyclase activity, and the induction of a too low Ca^{2+} influx.

ACT-ΔN482 hemolysin activates in J774A.1 cells a wounded membrane repair-like pathway involving exocytic and endocytic steps

To investigate whether mechanisms proposed to operate downstream from Ca^{2+} -dependent repair of large membrane pores were also implicated here, we performed several different assays in parallel. We explored by confocal microscopy and flow cytometry the cellular ACT-ΔN482 hemolysin localization (**Fig 6**). Representative confocal microscopy images taken from J744A.1 cells exposed for 10 min to two different ACT-ΔN482 hemolysin concentrations (1 and 10 nM) are shown in **Fig 6A**. When cells were exposed to the pore-forming protein ACT-ΔN482 hemolysin at 4°C the green fluorescence signal (monoclonal Ab anti-ACT 9D4) was detected only at the cell surface, with no detectable toxin labeling inside cells (**Fig 6A**). On the contrary, in cells incubated with this hemolysin at 37°C the green fluorescence signal was detected both at the plasma membrane and in the cell interior in a more punctuate form (**Fig 6A**). As endocytic processes are severely inhibited at low temperatures, these results were a first clue that ACT-ΔN482 was internalized by J744A.1 cells. Data from cell cytometry experiments reassured the above data, as showed a time-dependent toxin uptake, achieving about 40% internalization within 10-30 min after toxin treatment (**Fig. 6B**). Notably, the ACT-ΔN482 disappearance kinetics was parallel to the time-course in which cells became impermeable to PI, strongly supporting the idea that the most likely cause of the progressive cell membrane resistance to PI penetration is the elimination of ACT-ΔN482 hemolysin pores by endocytosis, and that this contributes to membrane resealing.

ACT-ΔN482 (2.5 nM) induced a time-dependent accumulation of β-hexosaminidase, a marker of lysosomal exocytosis [11] in the extracellular medium of toxin-treated macrophages (**Fig. 6C**) and in line with a role of lysosomal exocytosis in

membrane repair upon the hemolysin attack, in cells preincubated with bromoenol lactone (BEL; 20 μM) (Sigma) which blocks lysosomal exocytosis without interfering with Ca^{2+} influx [48]] and was reported to inhibit membrane repair in SLO-treated cells [49], the number of PI-positive cells notably increased as compared to the BEL-untreated cells (**Fig. 6D**). And consistent with this, inhibition of acid sphingomyelinase (ASM) with desipramine (DPA, 30 μM; Sigma), a potent pharmacological inhibitor of ASM [50,51], prominently affected the resealing capacity of the ΔN482-treated macrophages (**Fig. 6D**). Further, notable differences observed in the membrane ceramide content between the macrophages directly exposed to ACT-ΔN482 hemolysin (20 nM), and the cells that had been preincubated with DPA (**Fig 6E)** supported the conclusion of the involvement of ASM in the repair process. Of note, that in the ceramide quantification assay, we used thin layer chromatography (TLC), whose lower detection sensitivity required the use of higher toxin concentrations (20 nM). More sensitive methods such as immune-detection with an anti-ceramide antibody could not be used because of a cross-reaction of such Ab with the hemolysin itself (not shown).

DISCUSSION

Despite intense effort that has been input into investigating the interaction between RTX toxins and host cells during bacterial infection, our understanding on how RTX toxins insert and act into host cell membranes, and in turn, how host cells respond to the challenge of these toxins remains very limited.

This study scrutinizes the permeabilization elicited by the full length adenylate cyclase toxin (ACT) and its RTX hemolysin moiety, represented here by the mutant protein ACT-ΔN482, and dissects the response of target macrophages to the toxins attack.

We show that these two protein toxins permeabilize the target cell membrane very differently: while ACT-hemolysin induces a transient membrane permeabilization, which is reverted by activation of a Ca^{2+}- and ATP-dependent membrane repair pathway, the full length ACT toxin permeabilizes the cells irreversibly, leading eventually to cell death. Lack of enough Ca^{2+} influx and toxin-induced ATP depletion provide an explanation for the incapability of the ACT-treated cells to reseal the injured membrane.

Fluorescence microscopy and ICP-AES data demonstrate here that ACT-ΔN482-hemolysin can permeabilize the cell membrane of macrophages at concentrations <1.0 nM, inducing a rapid intracellular K^+ efflux, and also an extracellular Ca^{2+} entry (**Fig 2**). Moreover, our results with several inhibitors (PPADS, nifedipine and KT5720) of different kind of channels allow us to conclude that such permeabilization by ACT-ΔN482 is independent of the activation of L-type Ca^{2+} channels or purinergic channels, at least for-the ACT-ΔN482 hemolysin concentrations tested in the study (<2.5-5.0 nM), and so, the simplest and more reasonable explanation for such ions fluxes is, in principle, that the ACT-ΔN482 hemolysin forms K^+ - and Ca^{2+}-permeable pores into the cell membrane. This conclusion is reinforced by the finding here that upon ACT-ΔN482 hemolysin exposure the macrophage membrane becomes permeable to PI, which has a molecular mass of ≈644 Da and a diameter of ≈1.0 nm, in the same time scale, and same concentration range, that the fluxes of K^+ and Ca^{2+} ions are detected (**Figs 1 and 3**), while the membrane remains impermeable to LDH, and thus cells are expectedly alive (**Fig 3**). This is, the data indicate that upon cell binding, the ACT-hemolysin moiety may rapidly form K^+-, Ca^{2+}- and PI-permeable pores, but without inflicting massive collapse of the membrane permeability barrier (**Fig 3**). By contrast, pores formed by wt ACT in the macrophages membrane show marked differences relative to the ACT-ΔN482 hemolysin

pores, since, at the same concentration range, they appear to be permeable to K^+ ions, but initially PI-impermeable, and only slightly permeable to Ca^{2+} (**Figs. 1 and 2**). The most ready explanation for such differences might be the differences in the effective size of the pores formed by both toxins in the plasma membrane, since according to previous studies by others ACT pores would be of very small diameter (0.6-0.8 nm)[32], similar for example to the *Staphylococcus aureus* α-hemolysin pores, which are also permeable to K^+ but Ca^{2+}-impermeable [52]. Importantly, we reveal here that ACT-ΔN482 hemolysin permeabilizes the cell membrane "reversibly", and provide evidences demonstrating that the process of membrane integrity recovery depends on extracellular Ca^{2+} influx and ATP (**Figs. 3-5)**. Further, we provide ample evidence supporting that recovery of the membrane integrity involves consecutive steps of exocytosis and endocytosis (**Fig. 6**), likely initiated by lysosomal fusion with the damaged cell membrane, subsequent secretion to the extracellular medium of acid sphingomyelinase and concomitant local generation of ceramide, all of which ends in the endocytosis of the pore-ridden membrane, which re-establishes cell membrane impermeability and assures cell viability. Up to now, such a membrane repair mechanism, Ca^{2+} - and ATP-dependent, had only been reported for toxins forming beta-barrel pores into membranes, large pores such as streptolysin, perfringolysin, pneumolysin or listeriolysin [4,6] or lesions formed by the small β-pore forming phobalysin [7]; lesions by ACT and its homologous RTX toxins, in contrast, are presumably formed by insertion of amphipathic/ hydrophobic α-helices.

It is also notable our finding that the full length ACT at relatively low toxin concentrations (≤5.0 nM), inflicts in macrophages an irreparable membrane permeabilization (**Figs. 3 and 5**) which may ultimately lead to a progressive cell death, distinguishing hence from the "reversible or repairable" damage elicited by the ΔN482

hemolysin . We provide evidences here that, early after ACT pulse, the cell membrane becomes permeable to K^+ presumably due to ACT pores, and remains so, K^+-permeable, along the whole time until it becomes permeable also to PI and LDH (**Fig 5**). This rules out that the initial impermeability to PI observed in the ACT-treated macrophages, goes preceded by a rapid, (endocytosis-based), membrane resealing, but rather it is due to the permanence in the membrane of small K^+-permeable ACT pores, and thus it proves that ACT permeabilization is irreversible, and irreparable, and that cells become permeable to PI at the same or similar time that become permeable to LDH, this is when cells die. We postulate that this incapability of the macrophages treated with low ACT concentrations to eliminate the pores and so to reseal the injured membrane may be explained by the faint Ca^{2+} rise induced by ACT along with the ATP consumption by its AC activity, since as we have demonstrated here (**Fig 5**), and others had also previously noted [10,11], these two factors, Ca^{2+} and ATP are indispensable for activation of membrane repair processes in cells. From all these data it can be guessed that a "threshold concentration" of Ca^{2+} and likely of ATP may exist that are required for activation of calcium-based membrane repair pathways in cells, and so it could be anticipated that below such "threshold" amount, injury repairing would evolve to an unsuccessful task. Therefore it could be affirmed that not the particular affiliation with a structural family of PFT, α or β, but sufficient influx of calcium through the pores formed in the membrane, and enough energy (ATP) seems to be key for triggering rapid membrane repair.

We do not ignore that at the concentrations used in our assays (<5.0 nM) wt ACT generates important amounts of cAMP into the cells, in parallel to pore formation, that can induce cell toxicity [34]. But at this regard it was previously noted that it is the concomitant ATP depletion, and not directly the cAMP produced, the responsible for cell

dying [53] since a high cAMP level *per se* does not kill the ACT-treated cells [53] . However, as we have found here permeabilization of the cell membrane to K^+ and Ca^{2+} following ΔN482 hemolysin pulse also provokes a concomitant and abrupt ATP fall in cells (**Fig 7**); however, those cells do not die (remain LDH negative), very likely because they are capable to repair their membrane (there is Ca^{2+} influx) and can thus survive. From this, it can thus be reasonably postulated that a permanent membrane permeabilization (coming from incapability to reseal the injuries, what precludes the recovery of energy homeostasis) might be deleteriously enough so as to kill cells, though up to now cAMP production by the AC domain has been regarded as the only or main ACT cytotoxic effector at low sublytic toxin concentrations.

Given the high similarity among the ACT RTX-hemolysin moiety and toxins from the RTX family, it is enticing to surmise that a similar, Ca^{2+}-dependent, membrane repair mechanism might also operate for those pore-forming toxins. Full length wt ACT, by contrast, might have evolved causing apparently less serious membrane perturbations and escaping from control by the cellular wounded membrane repair response, and this, in turn, suggests that this toxin, in a low concentration physiological context, might use its pore-forming moiety primarily as a "molecular injector" to achieve the cell cytosol.

ACKNOWLEDGMENTS

Technical and human support provided by SGIker (Analytical and High-Resolution Microscopy in Biomedicine Service of UPV/EHU) and Rocío Alonso for excellent technical assistance are gratefully acknowledged. We also thank Prof A. Gómez-Muñoz for flow cytometry facilities and Dr. C. Angsuthanasombat and Dr. B. Powthongchin (Mahidol University, Thailand) for pCyaAC-PF plasmid.

This study was supported by grants from the Basque Goverment (Grupos Consolidados IT849-13 and IT1264-19) and grants from the Spanish Ministerio de Economía y Competitividad (BFU2014-53469P to M.T.A. A, and BFU-2017-82758-P (AEI/FEDER, UE) to H. O. A.E. was recipient of a fellowship from the University of the Basque Country (UPV/EH). D.G.B. was recipient of a fellowship from the Bizkaia Biophysics Foundation.

AUTHOR CONTRIBUTIONS

Conceived and designed the experiments: A.E., D.G.B., C.M., H. O. Performed the experiments: A.E., D.G.B , C.M.. Analysed the data: A.E., D.G.B, M.T.A., C.M., H.O. Wrote the paper: H. O.

COMPETING INTERESTS

The authors declare no competing financial interests.

REFERENCES

References

1. Bischofberger M, Iacovache I & Gisou Van Der Goot F (2012) Pathogenic pore-forming proteins: Function and host response. *Cell Host and Microbe* **12**, 266-275.

2. Dramsi S & Cossart P (2002) Listeriolysin O: A genuine cytolysin optimized for an intracellular parasite. *J Cell Biol* **156**, 943-946.

3. Husmann M, Beckmann E, Boller K, Kloft N, Tenzer S, Bobkiewicz W, Neukirch C, Bayley H & Bhakdi S (2009) Elimination of a bacterial pore-forming toxin by sequential endocytosis and exocytosis. *FEBS Lett* **583**, 337-344.

4. Walev I, Hombach M, Bobkiewicz W, Fenske D, Bhakdi S & Husmann M (2002) Resealing of large transmembrane pores produced by streptolysin O in nucleated cells is accompanied by NF-kappaB activation and downstream events. *FASEB J* **16**, 237-239.

5. Wolfmeier H, Schoenauer R, Atanassoff AP, Neill DR, Kadioglu A, Draeger A & Babiychuk EB (2015) Ca^{2+}-dependent repair of pneumolysin pores: A new paradigm for host cellular defense against bacterial pore-forming toxins. *Biochim Biophys Acta* **1853**, 2045-2054.

6. Gonzalez MR, Bischofberger M, Frêche B, Ho S, Parton RG & Van der Goot FG (2011) Pore-forming toxins induce multiple cellular responses promoting survival. *Cell Microbiol* **13**, 1026-1043.

7. Von Hoven G, Rivas AJ, Neukirch C, Meyenburg M, Qin Q, Parekh S, Hellmann N & Husmann M (2017) Repair of a bacterial small ß-barrel toxin pore depends on channel width. *mBio* **8**.

8. Los FCO, Kao C-, Smitham J, McDonald KL, Ha C, Peixoto CA & Aroian RV (2011) RAB-5- and RAB-11-dependent vesicle-trafficking pathways are required for plasma membrane repair after attack by bacterial pore-forming toxin. *Cell Host and Microbe* **9**, 147-151.

9. Keefe D, Shi L, Feske S, Massol R, Navarro F, Kirchhausen T & Lieberman J (2005) Perforin triggers a plasma membrane-repair response that facilitates CTL induction of apoptosis. *Immunity* **23**, 249-262.

10. Idone V, Tam C, Goss JW, Toomre D, Pypaert M & Andrews NW (2008) Repair of injured plasma membrane by rapid Ca2+-dependent endocytosis. *J Cell Biol* **180**, 905-914.

11. Tam C, Idone V, Devlin C, Fernandes MC, Flannery A, He X, Schuchman E, Tabas I & Andrews NW (2010) Exocytosis of acid sphingomyelinase by wounded cells promotes endocytosis and plasma membrane repair. *J Cell Biol* **189**, 1027-1038.

12. Thiery J, Keefe D, Saffarian S, Martinvalet D, Walch M, Boucrot E, Kirchhausen T & Lieberman J (2010) Perforin activates clathrin- and dynamin-dependent endocytosis, which is required for plasma membrane repair and delivery of granzyme B for granzyme-mediated apoptosis. *Blood* **115**, 1582-1593.

13. Ladant D & Ullmann A (1999) Bordetella pertussis adenylate cyclase: a toxin with multiple talents. *Trends Microbiol* **7**, 172-176.

14. Carbonetti NH & Artamonova GV (2005) Pertussis Toxin and Adenylate Cyclase Toxin Provide a One-Two Punch for Establishment of Bordetella pertussis Infection of the Respiratory Tract. *Infect Immun* , 2698-2703.

15. Welch RA (1991) Pore-forming cytolysins of gram-negative bacteria. *Mol Microbiol* **5**, 521-528.

16. Welch RA (2000) RTX toxin structure and function: A story of numerous anomalies and few analogies in toxin biology. *Curr Top Microbiol Immunol* **257**, 85-111.

17. Glaser P, Sakamoto H, Bellalou J, Ullmann A & Danchin A (1988) Secretion of cyclolysin, the calmodulin-sensitive adenylate cyclase-haemolysin bifunctional protein of Bordetella pertussis. *EMBO J* **7**, 3997-4004.

18. González-Bullón D, Uribe KB, Martín C & Ostolaza H (2017) Phospholipase A activity of adenylate cyclase toxin mediates translocation of its adenylate cyclase domain. *Proc Natl Acad Sci U S A* **114**, E6784-E6793.

19. González-Bullón D, Martín C & Ostolaza H (2018) Characterization of the intrinsic phospholipase A1 activity of bordetella pertussis adenylate cyclase toxin. *Toxins* **10**.

20. Berkowitz SA, Goldhammer AR, Hewlett EL & Wolff J (1980) Activation of prokaryotic adenylate cyclase by calmodulin. *Ann N Y Acad Sci* **356**, 360.

21. Hackett M, Guo L, Shabanowitz J, Hunt DF & Hewlett EL (1994) Internal lysine palmitoylation in adenylate cyclase toxin from Bordetella pertussis. *Science* **266**, 433-435.

22. Karst JC, Barker R, Devi U, Swann MJ, Davi M, Roser SJ, Ladant D & Chenal A (2012) Identification of a region that assists membrane insertion and translocation of the catalytic domain of Bordetella pertussis CyaA toxin. *J Biol Chem* **287**, 9200-9212.

23. Subrini O, Sotomayor-Pérez A-, Hessel A, Spiaczka-Karst J, Selwa E, Sapay N, Veneziano R, Pansieri J, Chopineau J, Ladant D & Chenal A (2013) Characterization of a membrane-active peptide from the bordetella pertussis CyaA toxin. *J Biol Chem* **288**, 32585-32598.

24. Masin J, Osickova A, Sukova A, Fiser R, Halada P, Bumba L, Linhartova I, Osicka R & Sebo P (2016) Negatively charged residues of the segment linking the enzyme and cytolysin moieties restrict the membrane-permeabilizing capacity of adenylate cyclase toxin. *Sci Rep* **6**.

25. Carbonetti NH (2010) Pertussis toxin and adenylate cyclase toxin: key virulence factors of Bordetella pertussis and cell biology tools. *Future Microbiol* **5**, 455-469.

26. Cannella SE, Ntsogo Enguéné VY, Davi M, Malosse C, Sotomayor Pérez AC, Chamot-Rooke J, Vachette P, Durand D, Ladant D & Chenal A (2017) Stability, structural and functional properties of a monomeric, calcium-loaded adenylate cyclase toxin, CyaA, from Bordetella pertussis. *Sci Rep* **7**.

27. Guermonprez P, Khelef N, Blouin E, Rieu P, Ricciardi-Castagnoli P, Guiso N, Ladant D & Leclerc C (2001) The adenylate cyclase toxin of Bordetella pertussis binds to target cells via the alpha(M)beta(2) integrin (CD11b/CD18). *J Exp Med* **193**, 1035-1044.

28. González-Bullón D, Uribe KB, Martín C & Ostolaza H (2017) Phospholipase A activity of adenylate cyclase toxin mediates translocation of its adenylate cyclase domain. *Proc Natl Acad Sci U S A* **114**, E6784-E6793.

29. Confer DL & Eaton JW (1982) Phagocyte impotence caused by an invasive bacterial adenylate cyclase. *Science* **217**, 948-950.

30. Bellalou J, Sakamoto H, Ladant D, Geoffroy C & Ullmann A (1990) Deletions affecting hemolytic and toxin activities of Bordetella pertussis adenylate cyclase. *Infect Immun* **58**, 3242-3247.

31. Rogel A & Hanski E (1992) Distinct steps in the penetration of adenylate cyclase toxin of Bordetella pertussis into sheep erythrocytes. Translocation of the toxin across the membrane. *J Biol Chem* **267**, 22599-22605.

32. Benz R, Hardie KR & Hughes C (1994) Pore formation in artificial membranes by the secreted hemolysins of Proteus vulgaris and Morganella morganii. *Eur J Biochem* **220**, 339-347.

33. Szabo G, Gray MC & Hewlett EL (1994) Adenylate cyclase toxin from Bordetella pertussis produces ion conductance across artificial lipid bilayers in a calcium- and polarity-dependent manner. *J Biol Chem* **269**, 22496-22499.

34. Hewlett EL, Donato GM & Gray MC (2006) Macrophage cytotoxicity produced by adenylate cyclase toxin from Bordetella pertussis: more than just making cyclic AMP! *Mol Microbiol* **59**, 447-459.

35. Knapp O, Maier E, Polleichtner G, Mašín J, Šebo P & Benz R (2003) Channel formation in model membranes by the adenylate cyclase toxin of Bordetella pertussis: Effect of calcium. *Biochemistry* **42**, 8077-8084.

36. Vojtova-Vodolanova J, Basler M, Osicka R, Knapp O, Maier E, Cerny J, Benada O, Benz R & Sebo P (2009) Oligomerization is involved in pore formation by Bordetella adenylate cyclase toxin. *FASEB J* **23**, 2831-2843.

37. Gray M, Szabo G, Otero AS, Gray L & Hewlett E (1998) Distinct mechanisms for K+ efflux, intoxication, and hemolysis by Bordetella pertussis AC toxin. *J Biol Chem* **273**, 18260-18267.

38. Uribe KB, Etxebarria A, Martín C & Ostolaza H (2013) Calpain-Mediated Processing of Adenylate Cyclase Toxin Generates a Cytosolic Soluble Catalytically Active N-Terminal Domain. *PLoS ONE* **8**.

39. Karst JC, Ntsogo Enguene VY, Cannella SE, Subrini O, Hessel A, Debard S, Ladant D & Chenal A (2014) Calcium, acylation, and molecular confinement favor folding of Bordetella pertussis adenylate cyclase CyaA toxin into a monomeric and cytotoxic form. *J Biol Chem* **289**, 30702-30716.

40. Martin C, Uribe KB, Gomez-Bilbao G & Ostolaza H (2011) Adenylate cyclase toxin promotes internalisation of integrins and raft components and decreases macrophage adhesion capacity. *PLoS One* **6**, e17383.

41. Rodríguez A, Webster P, Ortego J & Andrews NW (1997) Lysosomes behave as Ca2+-regulated exocytic vesicles in fibroblasts and epithelial cells. *J Cell Biol* **137**, 93-104.

42. Gray MC, Lee SJ, Gray LS, Zaretzky FR, Otero AS, Szabo G & Hewlett EL (2001) Translocation-specific conformation of adenylate cyclase toxin from Bordetella pertussis inhibits toxin-mediated hemolysis. *J Bacteriol* **183**, 5904-5910.

43. Masin J, Fiser R, Linhartova I, Osicka R, Bumba L, Hewlett EL, Benz R & Sebo P (2013) Differences in purinergic amplification of osmotic cell lysis by the pore-forming RTX toxins bordetella pertussis CyaA and actinobacillus pleuropneumoniae ApxIA: The role of pore size. *Infect Immun* **81**, 4571-4582.

44. Martin C, Gomez-Bilbao G & Ostolaza H (2010) Bordetella adenylate cyclase toxin promotes calcium entry into both CD11b+ and CD11b- cells through cAMP-dependent L-type-like calcium channels. *J Biol Chem* **285**, 357-364.

45. Wald T, Petry-Podgorska I, Fiser R, Matousek T, Dedina J, Osicka R, Sebo P & Masin J (2014) Quantification of potassium levels in cells treated with Bordetella adenylate cyclase toxin. *Anal Biochem* **450**, 57-62.

46. Skals M, Bjaelde RG, Reinholdt J, Poulsen K, Vad BS, Otzen DE, Leipziger J & Praetorius HA (2014) Bacterial RTX toxins allow acute ATP release from human erythrocytes directly through the toxin pore. *J Biol Chem* **289**, 19098-19109.

47. Eby JC, Gray MC, Warfel JM, Paddock CD, Jones TF, Day SR, Bowden J, Poulter MD, Donato GM, Merkel TJ & Hewlett EL (2013) Quantification of the adenylate cyclase toxin of bordetella pertussis in vitro and during respiratory infection. *Infect Immun* **81**, 1390-1398.

48. Rodríguez A, Webster P, Ortego J & Andrews NW (1997) Lysosomes behave as Ca2+-regulated exocytic vesicles in fibroblasts and epithelial cells. *J Cell Biol* **137**, 93-104.

49. Fensome-Green A, Stannard N, Li M, Bolsover S & Cockcroft S (2007) Bromoenol lactone, an inhibitor of Group V1A calcium-independent phospholipase A2 inhibits antigen-stimulated mast cell exocytosis without blocking Ca2+ influx. *Cell Calcium* **41**, 145-153.

50. Albouz S, Hauw JJ, Berwald-Netter Y, Boutry JM, Bourdon R & Baumann N (1981) Tricyclic antidepressants induce sphingomyelinase deficiency in fibroblast and neuroblastoma cell cultures. *Biomedicine* **35**, 218-220.

51. Kolzer M, Werth N & Sandhoff K (2004) Interactions of acid sphingomyelinase and lipid bilayers in the presence of the tricyclic antidepressant desipramine. *FEBS Lett* **559**, 96-98.

52. Walev I, Palmer M, Martin E, Jonas D, Weller U, Höhn-Bentz H, Husmann M & Bhakdi S (1994) Recovery of human fibroblasts from attack by the pore-forming a-toxin of Staphylococcus aureus. *Microb Pathog* **17**, 187-201.

53. Basler M, Masin J, Osicka R & Sebo P (2006) Pore-forming and enzymatic activities of Bordetella pertussis adenylate cyclase toxin synergize in promoting lysis of monocytes. *Infect Immun* **74**, 2207-2214.

FIGURE LEGENDS

Fig. 1. **Permeabilization of J774A.1 macrophages by ACT and ACT-ΔN482**.

A. FACS analysis of propidium iodide (PI) uptake by J774A.1 cells exposed to ACT (2.5 nM) and ACT-ΔN482 (2.5 nM) for 10 min at 37°C. The gated region in the histogram represents PI positive cells. Control cells were exposed to the same vehicle buffer under the same experimental conditions. The figure shows representative histograms from three independent experiments. **B**. Concentration dependence of cell permeabilization to PI by ACT and ACT-ΔN482. J774A.1 cells were treated for 10 min at 37° with increasing amounts of ACT or ACT-ΔN482, and then cells were stained for 4 min with PI (50μg/mL). PI uptake was determined by flow cytometry as described in *Experimental procedures*. Measurements were independently performed at least 3 times, with n=3 and results are presented as mean ± s.d.

Fig. 2. **ACT-ΔN482 hemolysin elicits permeability to K^+ and Ca^{2+} ions, whereas intact ACT at low concentrations permeabilizes the phagocytes only to K^+.** **A**. Intracellular [K^+] variations in J774A.1 cells exposed to three different ACT-ΔN482 concentrations (0.1, 0.25 and 1.0 nM). **B**. Intracellular [K^+] variations induced by ACT at three different concentrations (2.5, 5 and 30 nM). Variations of the intracellular [K^+] were quantified using the inductively coupled plasma atomic emission spectroscopy technique (ICP-AES) as described in *Experimental procedures*. **C.** Ca^{2+} dynamics in J774A.1 macrophages exposed to different concentrations of ACT-Δ482 hemolysin (1.0, 2.5 and 5.0 nM), or to ACT (1.0, 2.5, 5.0 and 30 nM) was determined by changes in the fluorescence of the Fura-2 Ca^{2+}-sensitive probe as described in *Experimental Procedures*. Proteins were added to the cells at t=200 s. Traces for each protein concentration correspond to the mean values of the measurements performed in at least 30 cells.

Fig. 3. **Phagocytes permeabilized by ACT-ΔN482 hemolysin reseal their plasma membrane, but permeabilization by full length ACT is not repaired**. **A**. Analysis by flow cytometry of propidium iodide uptake by J774A.1 cells exposed to ACT-ΔN482 by constant incubation (upper panel) or 5 min short incubation (pulse) (lower panel). PI uptake is indicative of cell membrane permeabilization, while PI exclusion indicates membrane resealing. **B**. Permeabilization and recovery of the plasma membrane integrity followed by PI uptake analysis after short exposure ("pulse") to ACT-ΔN482. **C.** Time course of permeability to PI of macrophages incubated for a short pulse with ACT (5 nM) or with ACT-ΔN482 (2.5 nM) **D**. Comparison between PI uptake and LDH release in J774.A1 cells incubated whit ACT (5 nM) for a short "pulse".

Fig. 4. **ACT-induced K^+ efflux as a function of time, following an initial short pulse with ACT.** Variations in the intracellular K^+ content induced by ACT (5.0 nM) or ACT-ΔN482 (2.5 nM) following a short pulse of 5 min were measured at different times (0', 5', 15', 30', 60' and 120') post-treatment. In the abscise axis, time = -5 min, corresponds to the K^+ content before toxin treatment, and time=0' corresponds to the time immediately after the 5' pulse (time post-treatment). Variations of the intracellular [K^+] were quantified using the inductively coupled plasma atomic emission spectroscopy technique (ICP-AES) as described in *Experimental procedures*. Measurements were independently performed at least 3 times, with n=3 and results are presented as mean ± s.d.

Fig. 5. **Extracellular Ca^{2+} influxand ATP are necessary for membrane resealing in phagocytes permeabilized by ACT-ΔN482 hemolysin**. **A**. Effects of the calcium chelator BAPTA-AM (50 μM) in the PI uptake of J774A.1 cells exposed to a short pulse (5 min) of ACT-ΔN482 (2.5 nM). Cells were pre-incubated with BAPTA-AM for 30 min. **B**. ATP was depleted by pre-treating cells for 1 h with 10 mM sodium azide and 20 mM 2-deoxyglucose (Sigma-Aldrich) in glucose-free HBSS and PI uptake assay was performed whit ACT-ΔN482 "pulse" incubation.

Fig. 6. **ACT-ΔN482 hemolysin is taken up by phagocytes** **A**. Analysis by confocal microscopy of the cellular localization of ACT-ΔN482 (in green) in J774A.1 cells treated with two different concentrations of the hemolysin (1.0 and 10 nM) for 5 min, at two different temperatures, 4°C and 37 °C. Cell nuclei are stained with Hoechst (in blue). **B**. Percentage of ACT-ΔN482 (5 nM) internalization into J774A.1 as a function of the incubation time, determined byflow cytometry as described under Materials and Methods section. **C**. Determination of lysosomal exocytosis in cells exposed to a short pulse (5 min) of ACT-ΔN482 (2.5 nM) measured as the release of the lysosomal enzyme β-hexosaminidase after different times of toxin treatment. **D.** Effect of desipramine (DPA), an inhibitor of acid sphingomyelinase, or bromoenol lactone (BEL) on the PI-uptake by J774A.1 cells exposed to a short pulse (5 min) of ACT-ΔN482 (5 nM). Cells were preincubated with DPA (30 μM) and BEL (20 μM) for 30 min. After that time the medium was removed and PI uptake assayed as described in *Experimental Procedures*. All measurements were independently performed at least 3 times, with n=3 unless otherwise stated, and results are presented as mean ± s.d. Levels of significance were determined by a two-tailed Student´s t test, and a confidence level of greater than 95% ($p<0.05$) were used to establish statistical significance.

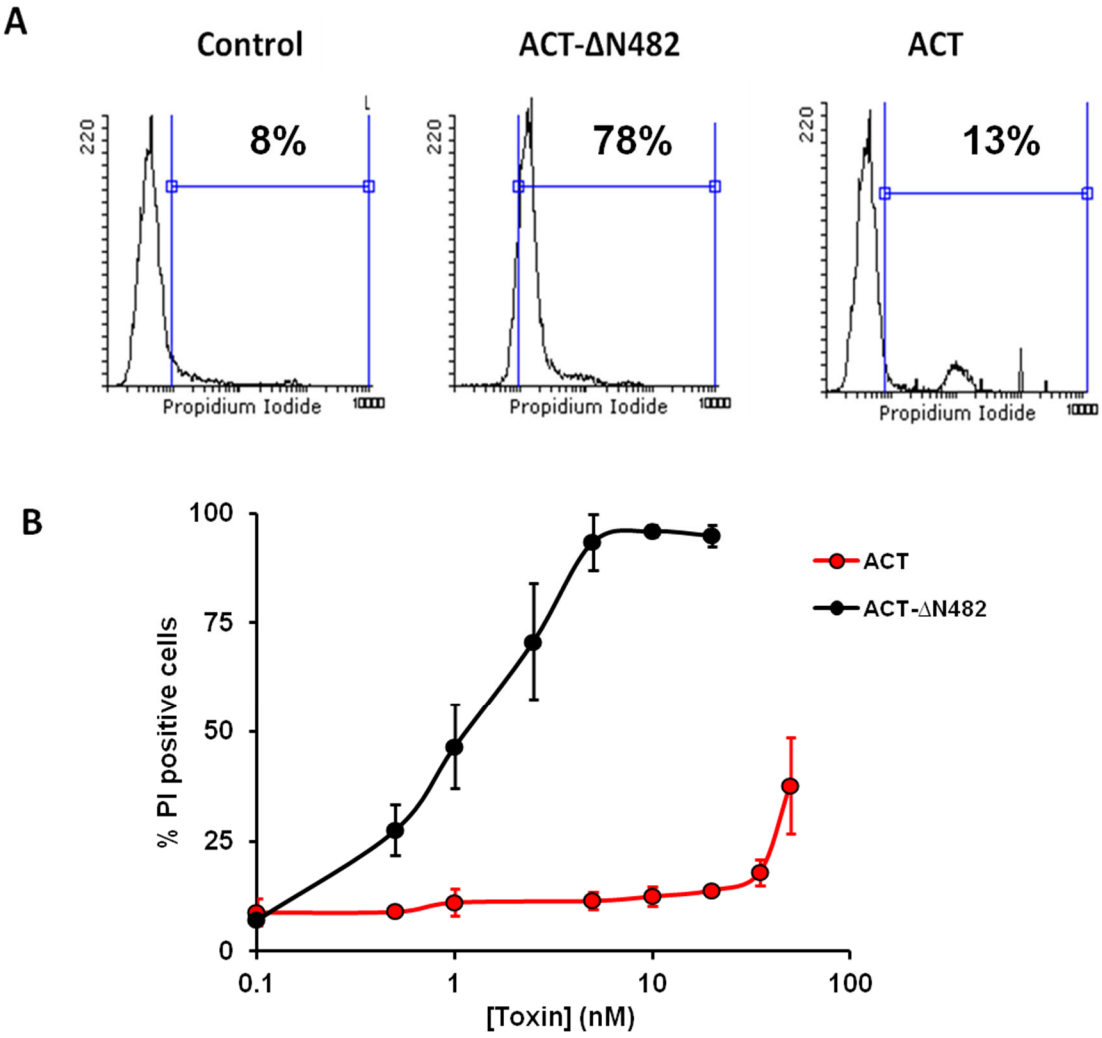
A
Control
ACT-ΔN482
ACT
8%
78%
13%
220
Propidium Iodide
B
% PI positive cells
100
75
50
25
0
0.1
1
10
100
[Toxin] (nM)
ACT
ACT-ΔN482

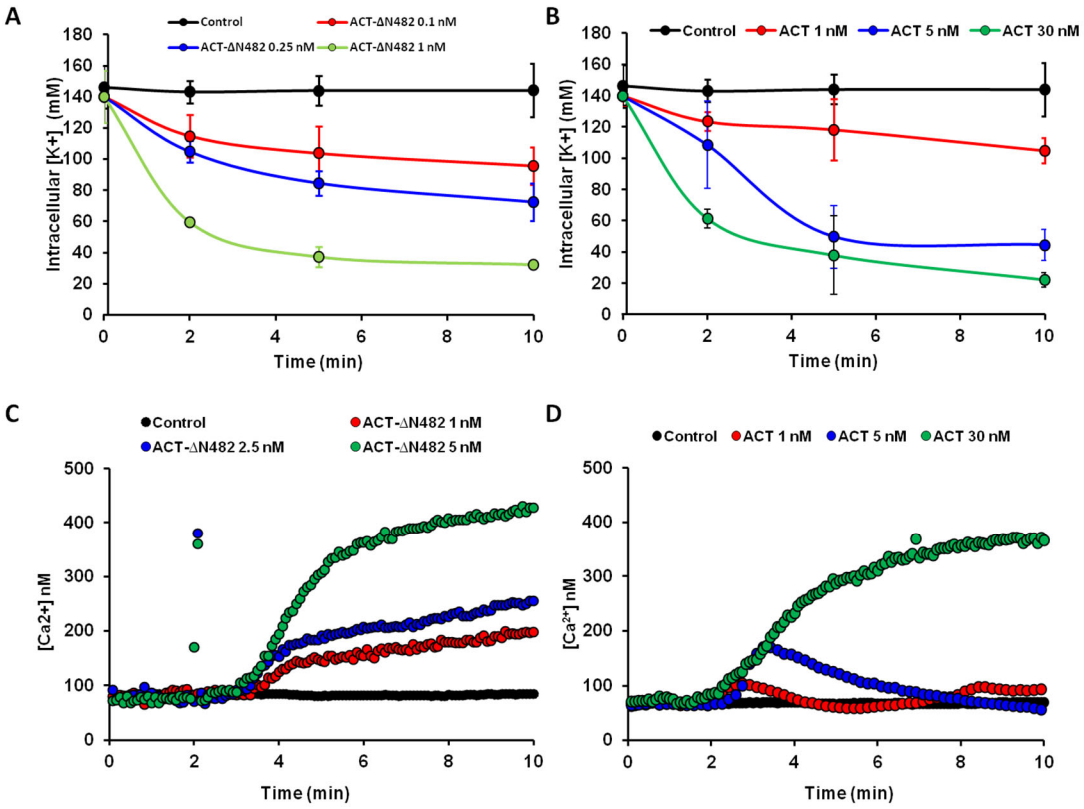
A
Control
ACT-ΔN482 0.1 nM
ACT-ΔN482 0.25 nM
ACT-ΔN482 1 nM
Intracellular [K+] (mM)
Time (min)
B
Control
ACT 1 nM
ACT 5 nM
ACT 30 nM
Intracellular [K+] (mM)
Time (min)
C
Control
ACT-ΔN482 1 nM
ACT-ΔN482 2.5 nM
ACT-ΔN482 5 nM
[Ca2+] nM
Time (min)
D
Control
ACT 1 nM
ACT 5 nM
ACT 30 nM
[Ca2+] nM
Time (min)

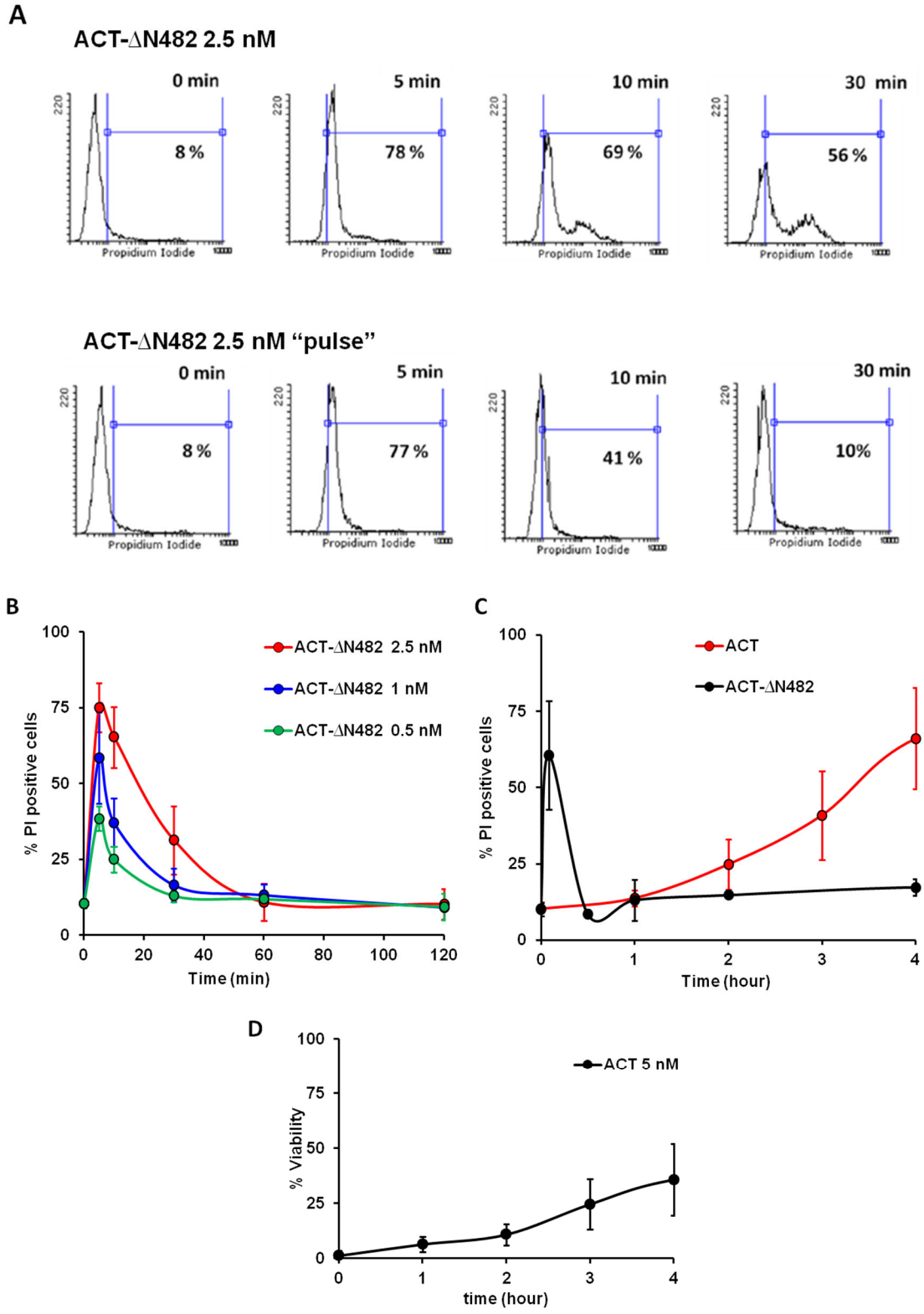
A
ACT-ΔN482 2.5 nM
0 min
8 %
5 min
78 %
10 min
69 %
30 min
56 %
Propidium Iodide
ACT-ΔN482 2.5 nM "pulse"
0 min
8 %
5 min
77 %
10 min
41 %
30 min
10%
B
ACT-ΔN482 2.5 nM
ACT-ΔN482 1 nM
ACT-ΔN482 0.5 nM
% PI positive cells
Time (min)
C
ACT
ACT-ΔN482
% PI positive cells
Time (hour)
D
ACT 5 nM
% Viability
time (hour)

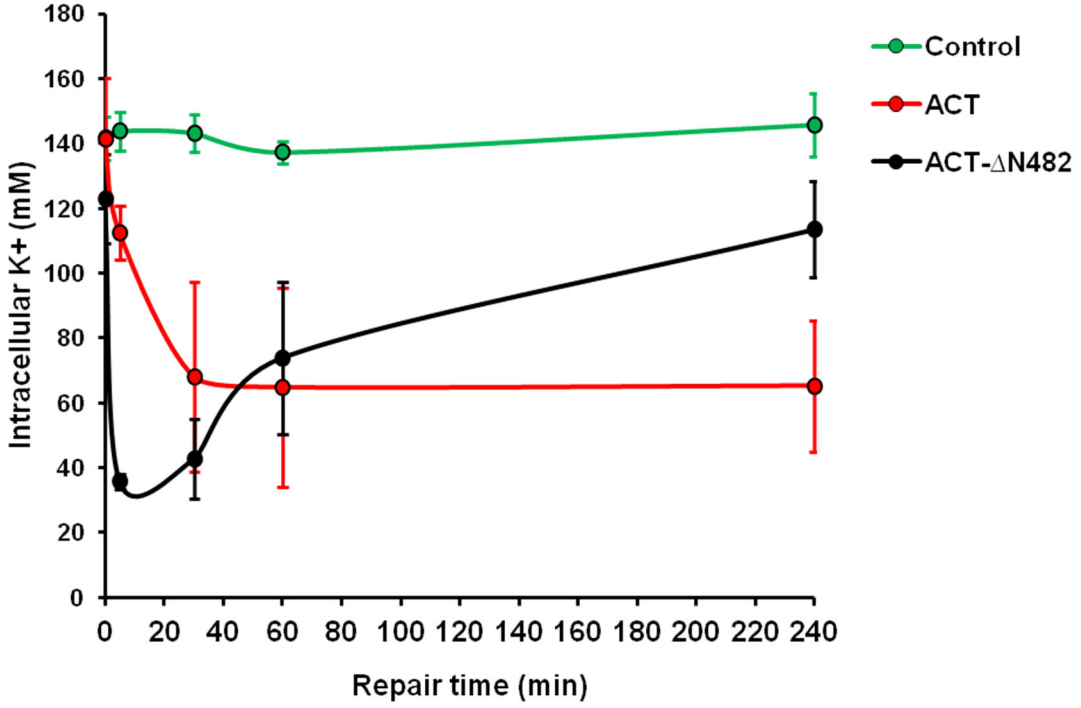
Intracellular K+ (mM)
180
160
140
120
100
80
60
40
20
0
0 20 40 60 80 100 120 140 160 180 200 220 240
Repair time (min)
Control
ACT
ACT-ΔN482

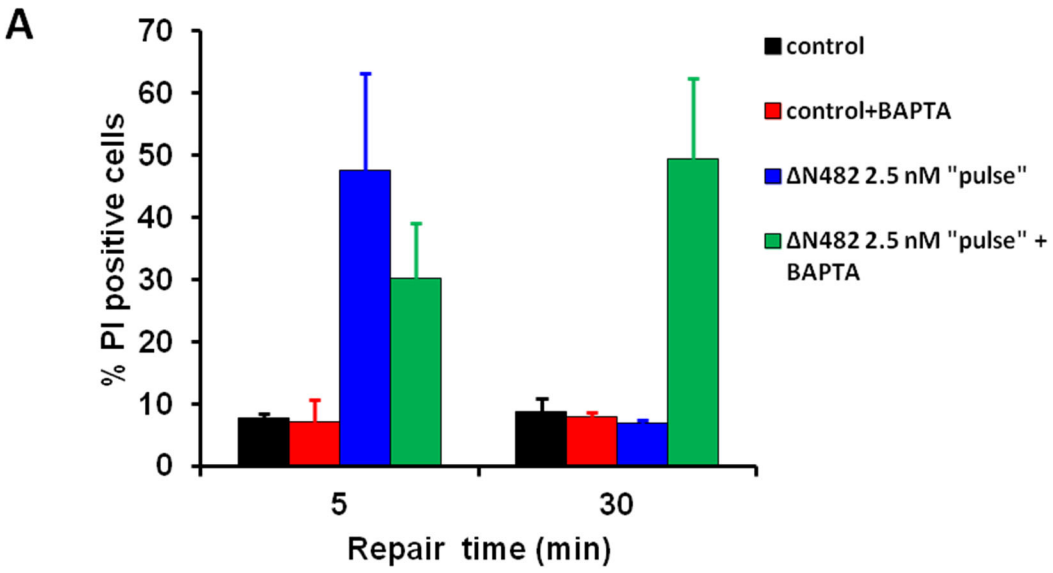
A
70
60
50
40
30
20
10
0
% PI positive cells
5
30
Repair time (min)
control
control+BAPTA
ΔN482 2.5 nM "pulse"
ΔN482 2.5 nM "pulse" + BAPTA

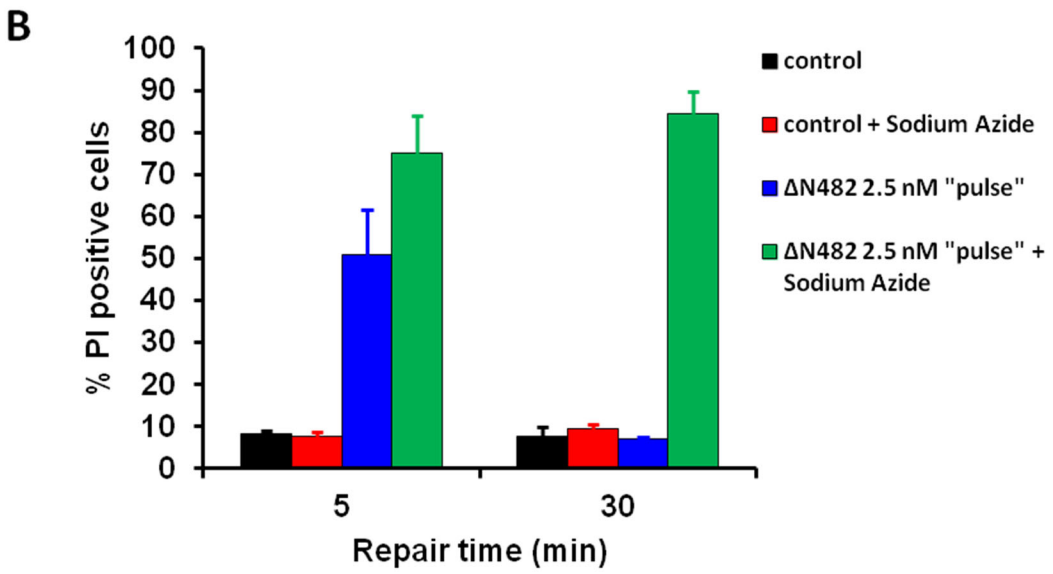
B
100
90
80
70
60
50
40
30
20
10
0
% PI positive cells
5
30
Repair time (min)
control
control + Sodium Azide
ΔN482 2.5 nM "pulse"
ΔN482 2.5 nM "pulse" + Sodium Azide

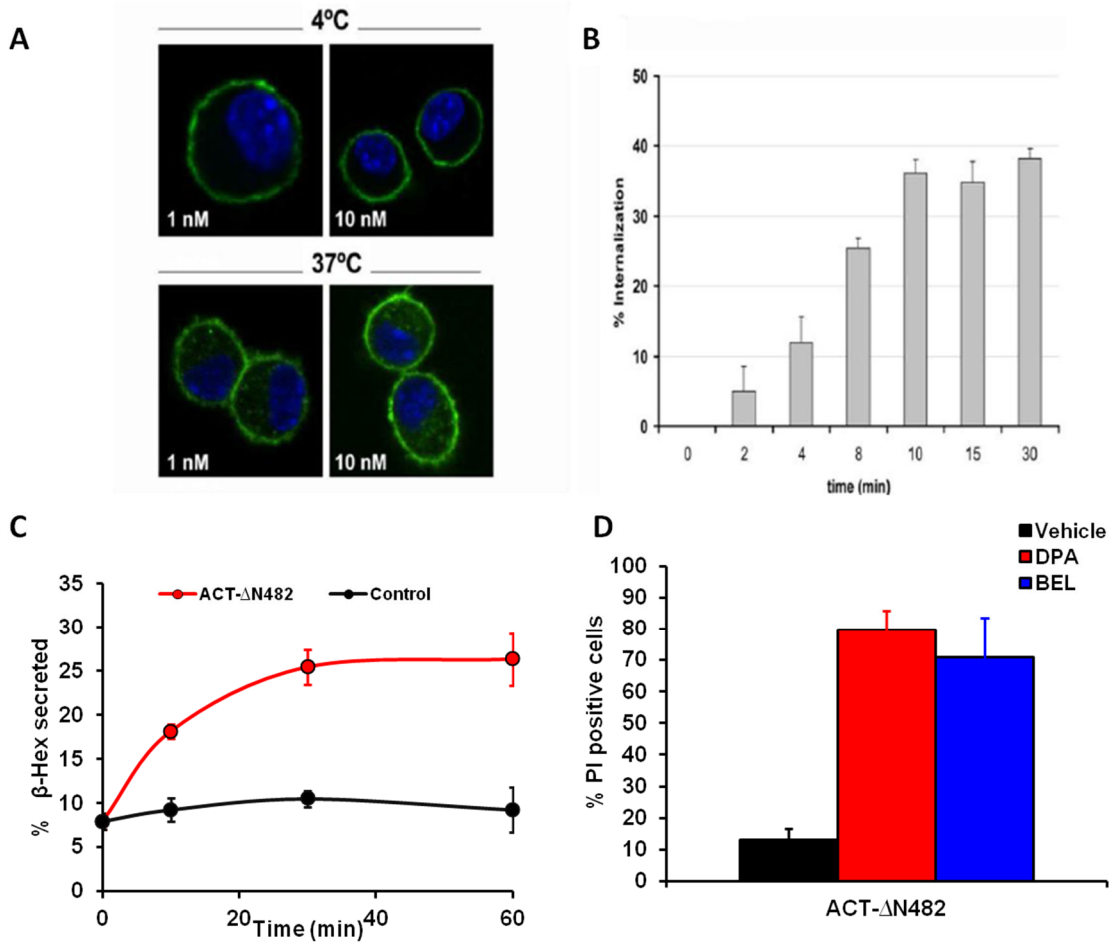
A
4°C
1 nM
10 nM
37°C
1 nM
10 nM
B
% Internalization
time (min)
0
2
4
8
10
15
30
C
ACT-ΔN482
Control
% β-Hex secreted
Time (min)
D
Vehicle
DPA
BEL
% PI positive cells
ACT-ΔN482

SUPPLEMENTARY INFORMATION

Manuscript Title: *Irreversible versus repairable membrane poration: differences in permeabilization elicited by Bordetella Adenylate Cyclase Toxin and its hemolysin domain in macrophages*

By Asier Etxaniz, David González-Bullón, César Martín, Maria Teresa Alonso and Helena Ostolaza

SUPPLEMENTARY FIGURE LEGENDS

Supplementary Fig. S1. Dose-dependent hemolysis by ACT-ΔN482 hemolysin and wt ACT on sheep erythrocytes. A standardized suspension of erythrocytes (≈5 x 10^8 cells/ml) was incubated with different ACT-ΔN482 hemolysin and wt ACT concentrations at 37°C and for 4h. After that time control cells and toxin-treated cells were centrifuged, and absorbance at 412 nm of the resultant supernatant was measured in a spectrofotometer. Percentage of hemolysis was calculated as describe in the section of *Materials and Methods* using as 100% lysis the absorbance value of a cell suspension to which TX-100 (0.1 % v/v) was added. Data depicted correspond to three independent experiments and mean values ±standard deviations are represented.

Supplementary Fig. S2. ACT permeability to K^+ is independent of calcium entry by L-type calcium channels. J774.A1 cells were preincubated with nifedipine (10 μM) or KT5720 (56 μM) two inhibitors of PKA-dependent L-type calcium channels, for 30 min at 37° C. After that time medium was removed and cells were exposed to ACT (5 nM) and measurement of intracellular K^+ was made as explained in *Experimental procedures*.

Supplementary Fig. S3. ACT-ΔN482 hemolysin permeability to Ca^{2+} is independent of PKA and L-type calcium channels. J774.A1 cells were preincubated with nifedipine (10 μM) or KT5720 (56 μM) 30 min. After that time medium was removed and cells were exposed to different concentrations of ACT-ΔN482 and measurement of intracellular Ca^{2+} was made as explained in *Experimental procedures*.

Supplementary Fig. S4. Effect of PPADS on the influx of Ca^{2+} induced by the ACT-ΔN48 hemolysin in macrophages. J774.A1 cells were preincubated for 10 min with pyridoxalphosphate-6-azophenyl-2',4'-disulfonic acid (PPADS) (20, 100 and 200 μM), a selective antagonist of P2X-type purinergic channels, and then measurement of intracellular Ca^{2+} was made upon treatment of cells with the hemolysin (2.5 nM), as explained in *Experimental procedures*.

Supplementary Fig. S5. PI uptake assay with PI present during toxin incubation. J774A.1 cells were treated with ACT-ΔN482 (2,5 nM) in short time (5 min) and medium was washed and replaced with medium with PI (50 μg/ml) for 30'. PI uptake was analyzed in flow cytometry as explained in *Experimental procedures*. Results were compared with assay in same conditions but whit PI added at the end of the incubation time.

Supplementary Fig. S6. PI uptake and LDH release in J774A.1 cell exposed to ACT-ΔN482. Cells were exposed to ACT-ΔN482 (2.5 nM) 5 min incubation at 37ºC and then the medium was washed with PBS and replace with DEMEN in PI uptake assay and Optimen in

LDH assay. Pi uptake and LDH release were monitored as described in *Experimental procedures.*

Supplementary Fig. S7. Ceramide generation by lysosomal acid sphingomyelinase in macrophages treated with ACT-ΔN482. A. Quantification by thin layer chromatography (TLC) and liquid scintillation counting of the ceramide content in the plasma membrane of control cells (control), cells treated with ACT-ΔN482 (20.0 nM) for 10 min at 37°C , or cells preincubated with desipramine (30 μM, 60 min), an inhibitor of acid sphingomielynase, and then with the hemolysin. All measurements were independently performed at least 3 times, with n=3 unless otherwise stated, and results are presented as mean ± s.d. Levels of significance were determined by a two-tailed Student´s *t* test, and a confidance level of greater than 95% ($p<0.05$) were used to establish statistical significance.

Supplementary Fig. S8. Determination of the intracellular ATP concentration, upon macrophage treatment with ACT or ACT-ΔN482. J774A.1 macrophages at confluency were exposed to wt ACT or ACT-ΔN482 at 1 nM concentration, 37°C, and the intracellular ATP content was then determined. [ATP] values are expressed as values relative to the ATP amount of untreated cells in HBSS vehicle buffer. ATP was determined using the Kinase-Glo® Luminescent Kinase assay kit (Promega, Spain).

Supplementary Fig. S9. Control of secondary antibodies alone in the confocal assay for cellular localization of ACT-ΔN482. Cells were grown to sub-confluency on to 12 mm diameter glass coverslips placed into the wells of a 24-well plate. Control cells were treated with vehicle buffer, then fixed for 10 min with 3.7% paraformaldehyde and permeabilized with acetone at –20 °C. Then samples were incubated with the appropriate primary antibodies anti-ACT 9D4 monoclonal antibody (Santa Cruz Biotechnology Inc, Germany) or anti-CD11b antibody (RM 280, Invitrogen) for 1 h, followed by incubation with Texas Red- or FITC-conjugated corresponding secondary antibodies.

Supplementary Fig S1

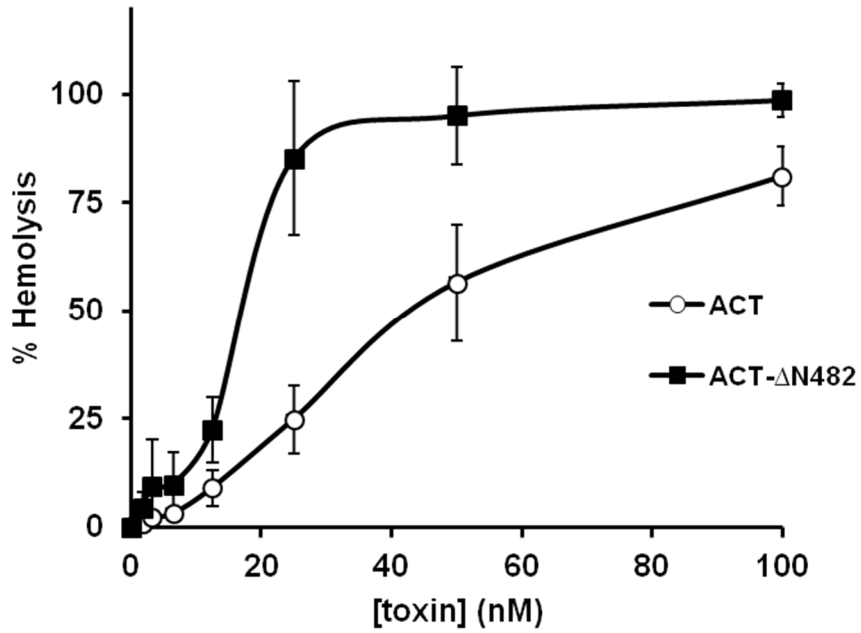

Supplementary Fig. S2

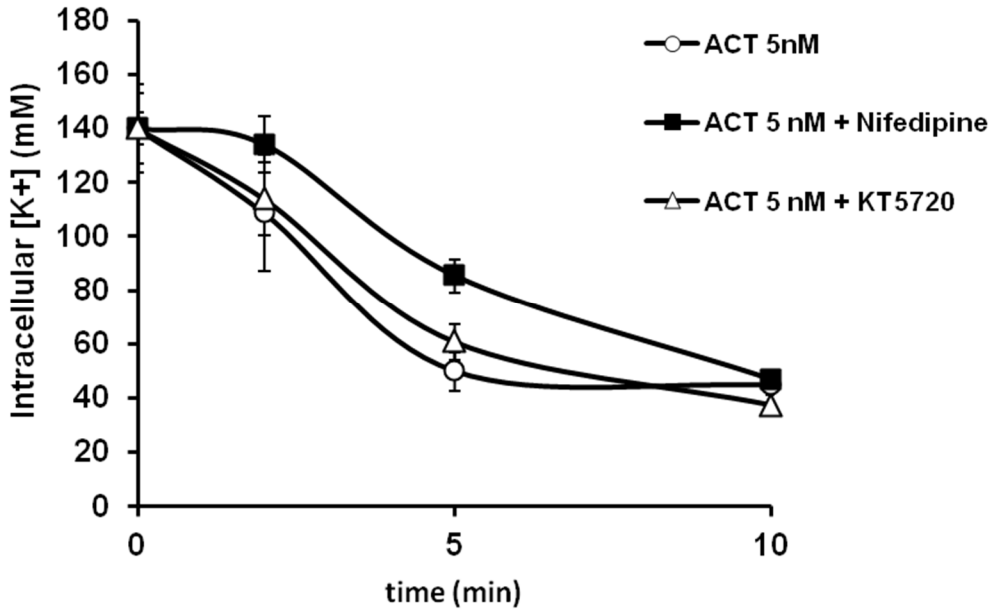

Supplementary Fig. S3

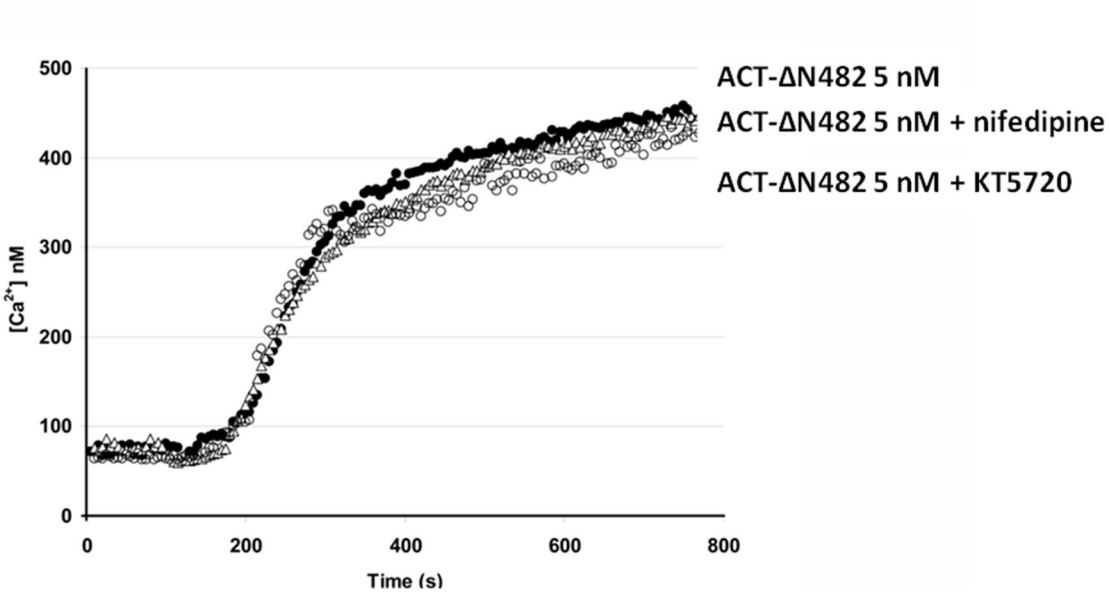

Supplementary Fig. S4

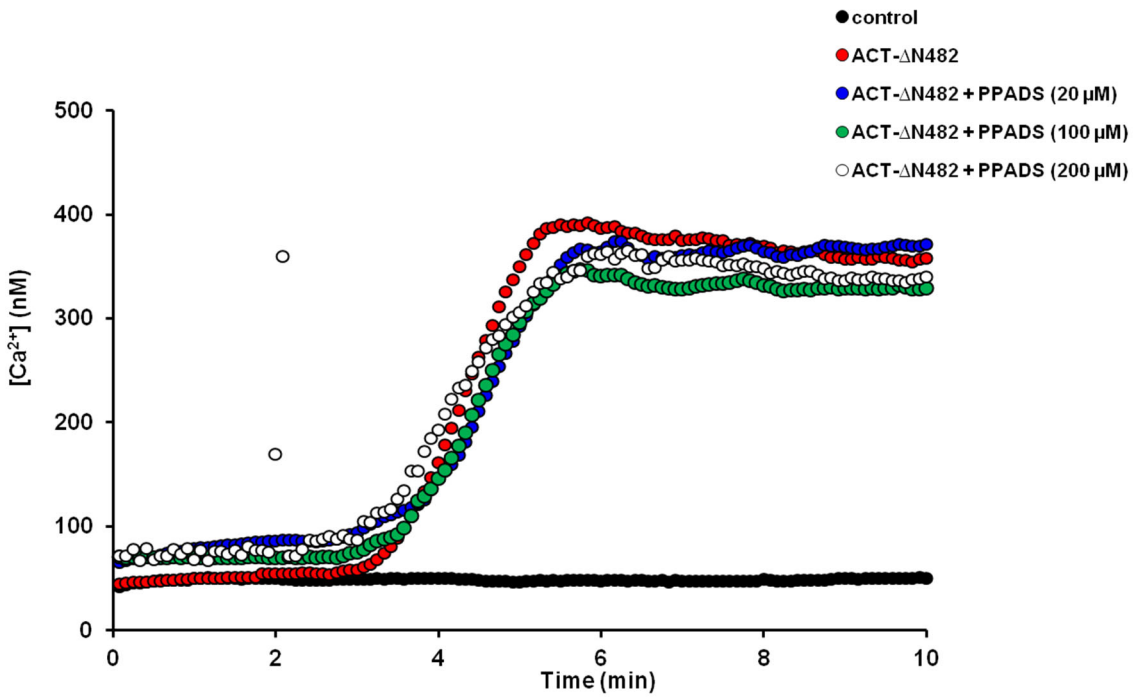

Supplementary Fig. S5

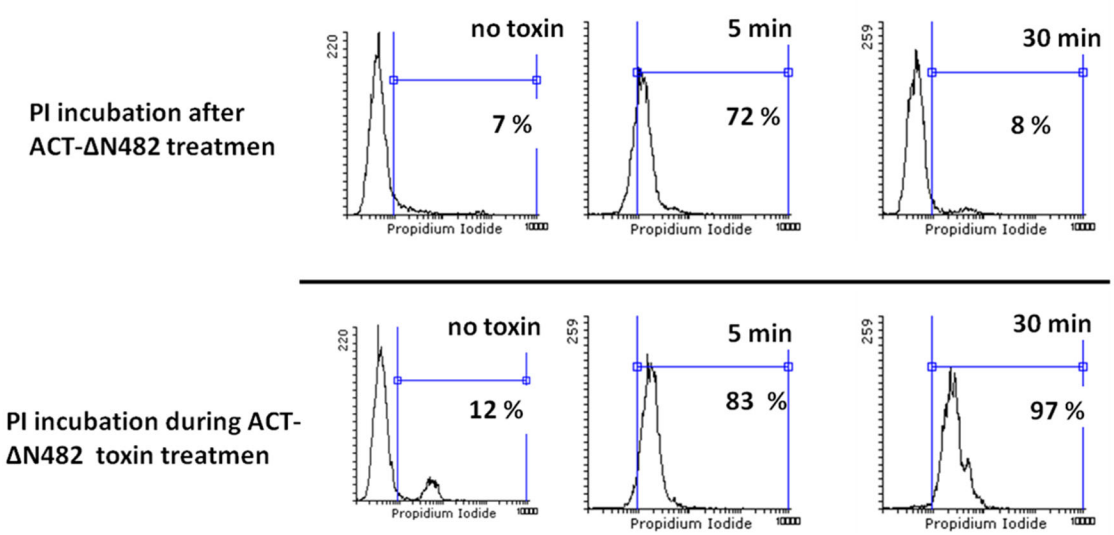

Supplementary Fig. S6

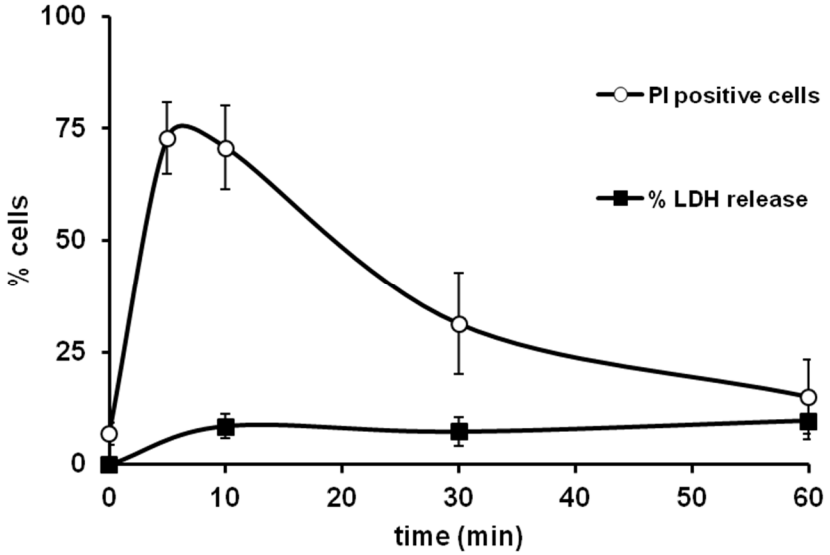

Supplementary Fig. S7

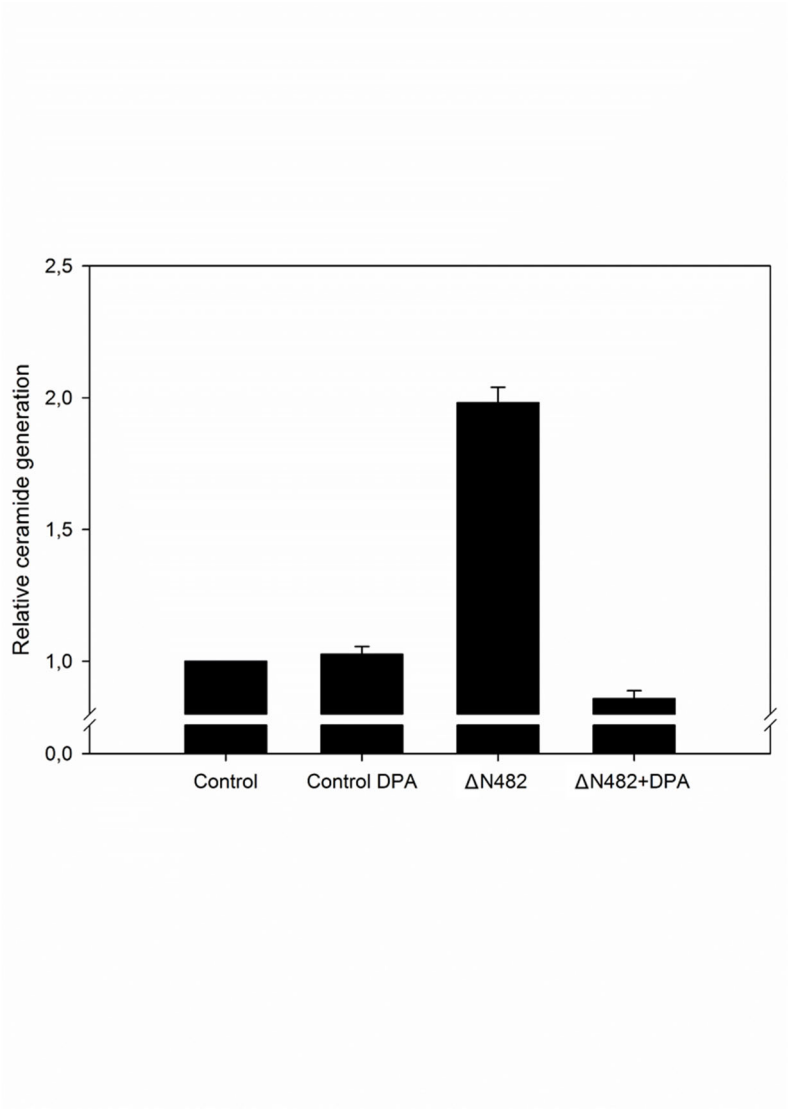

Supplementary Fig S8

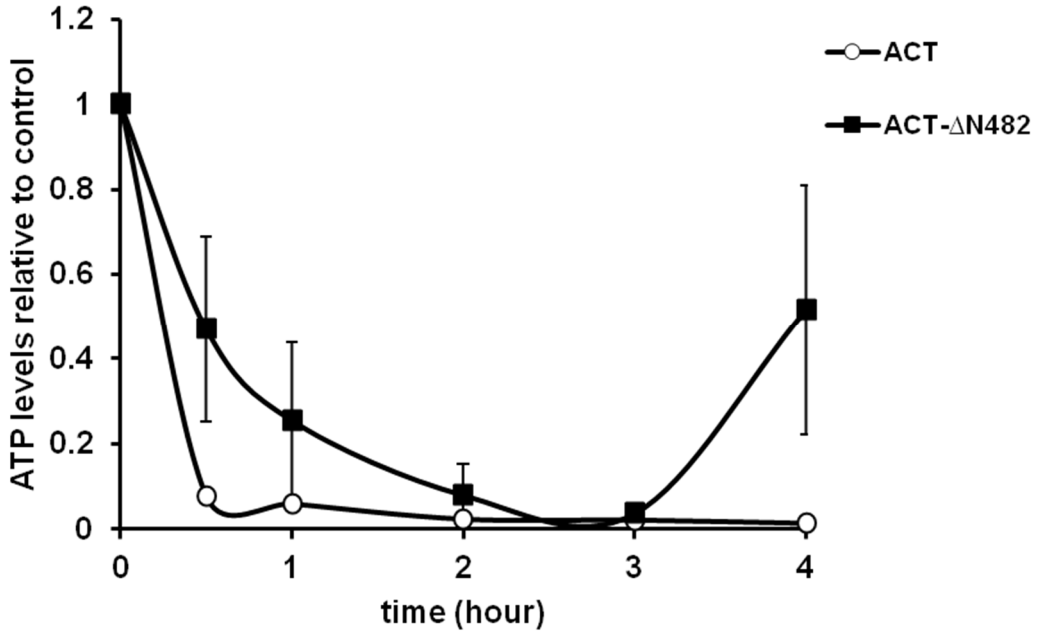

Supplementary Fig S9